Journal of Theoretical and Applied Vibration and Acoustics 3(1) 15- 40(2017)

I S A V

Journal of Theoretical and Applied Vibration and Acoustics

journal homepage: http://tava.isav.ir

Automatic formulation of falling multiple flexible-link robotic manipulators using 3×3 rotational matrices

Ali Mohammad Shafei *

Assistant Professor, Department of Mechanical Engineering, Shahid Bahonar University of Kerman, Kerman, Iran

ARTICLE INFO

Article history:
Received 15 January 2016

Received in revised form
28 October 2016

Accepted 4 November 2016

Available online 15 March 2017

Keywords:
Recursive formulation

Gibbs-Appell

Impact phase

Flying phase

3×3 rotational matrices

ABSTRACT

In this paper, the effect of normal impact on the mathematical modeling of flexible multiple links is investigated. The response of such a system can be fully determined by two distinct solution procedures. Highly nonlinear differential equations are exploited to model the falling phase of the system prior to normal impact; and algebraic equations are used to model the normal collision of this open-chain robotic system. To avoid employing the Lagrangian method which suffers from too many differentiations, the governing equations of such complicated system are acquired via the Gibbs-Appell (G-A) methodology. The main contribution of the present work is the use of an automatic algorithm according to 3×3 rotational matrices to obtain the system's motion equations more efficiently. Accordingly, all mathematical formulations are completed by the use of 3×3 matrices and 3×1 vectors only. The dynamic responses of this system are greatly reliant on the step sizes. Therefore, as well as solving the obtained differential equations by using several ODE solvers, a computer program according to the Runge-Kutta method was also developed. Finally, the computational counts of both algorithms i.e., 3×3 rotational matrices and 4×4 transformation matrices are compared to prove the efficiency of the former in deriving the motion equations.

* Corresponding author.

E-mail address: shafei@uk.ac.ir (A. M. Shafei)

http://dx.doi.org/10.22064/tava.2017.35085.1032

1. Introduction

When a mechanical system is subjected to applied impulses or the constraints on the system are abruptly varied, the velocity of the components in the system changes so rapidly that the duration of the process may be considered to be instantaneous. The mathematical modeling of ground collision in open chain robotic systems constructed of flexible links has diverse applications. For example, in the dynamic modeling of biped robotic systems, it is essential to know the dynamic responses of the system at the impact moments. In fact, the viscoelastic properties of human muscles that cover the bones justify the use of flexible links to model the bipedal robotic systems.

Unlike the classical problem of collision between two objects, a small amount of literature exists about the impact phenomenon in robotic systems. In an early study of this subject, Wittenburg [1] employed the Newton-Euler's methodology to obtain the governing equations at impact moments. Chang and Peng [2] exploited the Kane's formulation to investigate the impulsive motion in robotic systems by considering four various kinds of impulsive constraints. Mathematical modeling of frictional impacts in robotic manipulators have been studied by Hurmuzlu and Marghitu [3]. They developed three dynamical models for the coefficient of restitution according to the Newton's model of restitution. Rodriguez and Bowling [4] presented multi-point models of impact in rigid body systems. In this work, the effect of friction was also considered. The dynamic behavior of robotic manipulators with flexible joints colliding with their confining walls has been studied by Mahmoodi et al. [5]. In their paper, an adaptive controller is suggested to accomplish trajectory tracking of this robotic system. Shafei and Shafei [6] studied the effects of impact in open-chain robotic systems with flexible links. To simulate the conditions under which a single flexible link strikes with multiple flat confining walls, they employed the Newton's impact law. However, the chief objective of all the aforementioned studies has been to better the modeling of impact in robotic manipulators with finite numbers of rigid or flexible links; and robotic systems with many degrees of freedom have not been considered.

The two most important problems in the kinematic modeling of flexible robotic arms with impact phenomenon are: 1) How to model the impact moment between a flexible manipulator and the ground? and 2) How to capture an object by a flexible robotic arm with the least mechanical vibrations? Both of these impulsive events have involved many researchers [7-12]. The derivation of motion equations of elastic robotic arms, which encompass both aforementioned types of impulsive constraints, can be found in the works of Khulief and Shabana [13]. In this study, The FEM is utilized to model the elastic properties of the links for which the assumptions of Timoshenko Beam Theory (TBT) hold. A mathematical model was proposed by Yigit et al. [14] to study the dynamic responses of a rotating flexible beam with impact. Another model based on the Hertzian contact law, was proposed by the same authors for impact modeling [15]. However, because of system complexity, only one of the links was assumed to be flexible. Also, one may refer to the work of Chapnik et al. [16] in which the motion of a single flexible beam under impact loading was simulated by evaluating the proper initial conditions. Then, the obtained results from the computer simulation were compared to the measured data from the experimental setup. For more studies, one may refer to [17] where a literature review about impact in the dynamics of flexible robotic systems has been performed by Khulief.

The two chief questions in multi-flexible-link robotic manipulators with impulsive constraints are: 1) How to construct a valid elasto-dynamic model with the acceptable computational counts, and 2) How to incorporate the algebraic equations of this multi-flexible-link robotic arm into the relevant differential equations. In most of mechanical systems, it is essential to model the system as precise as possible. When more bodies are employed in dynamic modeling a robotic system, the mathematical operations needed to obtain the motion equations grow rapidly. Therefore, it is crucial to exploit an automatic algorithm to derive the motion equations, as fast as possible. There are many formulations that are effective in deriving the governing equations of open-chain robotic systems [18-24]. A comprehensive literature survey of the different recursive algorithms for elastic robotic manipulators may be found in [25]. Nevertheless, the stress of this paper is on the Gibbs-Appell formulation which has been used the least among the other method. Recently, Korayem and Shafei effectively applied this methodology for systematic formulation of flexible robotic arms [26-28], mobile robotic manipulators [29-31] and manipulators with revolute-telescopic joints [32, 33]. However, in none of these works the effects of impact between a manipulator and the ground have been considered.

The governing motion equations of robotic arms consisting of the unilateral constraints have formerly been fully formulated. The finite and impulsive motions of robotic arms with impacts can be characterized by differential and algebraic equations, respectively. However, the implementation of these differential-algebraic equations is restricted by significant computational load especially when the number of shape functions used to model the elastic properties of the flexible links increases. Consequently, researchers have concentrated to better the algorithms in order to simulate more complicated robotic systems with impact phenomenon. Förg et al. [34] suggested an algorithm for robotic systems with several constraints to treat many impacts. An $O(n)$ recursive algorithm according to the Projection Equation was offered by Gattringer et al. [35]. By using the Dirac delta functions, Tlalolini et al. [36] modeled the external forces originating from the collision of a thirteen-link humanoid robotic system with the ground. They exerted a Newton-Euler formulation in recursive form to extend an optimization algorithm for specifying the optimal cyclic gaits of the robot. Also, in the work of Shafei and Shafei [37], the mathematical model of multi-flexible-links subjected to impact was extracted in a symbolic format by employing the Gibbs-Appell formulation and 4×4 transformation matrices. However, despite using compact formulas in their work, the developed algorithm had a high computational complexity. Anyway, in all of the above-mentioned studies, the results of the impact model that should be exploited to characterize the generalized velocities of the system after impact moment, have not been formulated by an efficient algorithm with the least number of mathematical operations.

The focus of this paper is about symbolic derivation of multi-flexible-link robotic arms in finite and impulsive motions. So, this paper is formed as follows: Section 2 explains the kinematics of the system under study. The dynamics of the system, containing the construction of its global inertia matrix and global RHS vector in the flight phase and also the construction of the Jacobian matrix in the impact phase are presented in Section 3. The results of two computer simulations are presented in Section 4 to prove the efficiency of the proposed algorithm. Finally, the concluding remarks are summarized in Section 5 and the merits of the proposed method are highlighted.

2. Kinematics of a falling down multi-flexible link

2.1. System specifications

This section presents the kinematics of a planar robotic arm which constructed by flexible links and floated through the space. Link $(i-1)$ and Link (i) of this robotic system are depicted in Fig. 1. Two moving frames $(x_{i,1}x_{i,2}x_{i,3}, \hat{x}_{i,1}\hat{x}_{i,2}\hat{x}_{i,3})$ are assigned to each elastic link according to the forthcoming rules. $x_{i,1}x_{i,2}x_{i,3}$ is the moving frame for the i^{th} link that its origin is located at the start of this body; the $x_{i,1}$ axis is along the link when it is undeformed and the $x_{i,3}$ axis is aligned the joint axis. On the other hand, the origin of $\hat{x}_{i,1}\hat{x}_{i,2}\hat{x}_{i,3}$ moving frame is situated to the end of this link and its orientation is precisely the same as the $x_{i,1}x_{i,2}x_{i,3}$ moving frame, when this link has no deformation. Finally, ${}^{ref}X_1\,{}^{ref}X_2\,{}^{ref}X_3$ is the coordinate system which is devoted to the ground, as the global reference frame. In this paper, it is supposed that the manipulator has a moving base and consequently can easily move. So, the position and velocity of O_1 with respect to the inertia reference frame are respectively denoted by X_j and $\dot{X}_j$, where $j=1,2$. It is emphasized, the elastic attributes of the flexible links (i.e., modulus of elasticity E_i and modulus of rigidity G_i), mass per unit length (μ_i) and mass moment of inertia per unit length (J_i') are assumed to be isotopic along the links. Here, the elastic property of each link is modeled with the same number of shape functions (m). So, the degree of freedom (D.O.F) for the system is: $DOF = n + nm + 2$ where n D.O.F are related to the joint angles (q_j), nm D.O.F of the system are related to the small deflections of the links (δ_{ij}) and the remaining two D.O.F are associated with the position of the start point (O_1) with respect to the global coordinate system (X_j).

2.2. Kinematic equations

In Fig. 1, a differential element, Q, is demonstrated. The location of this differential element with respect to the $x_{i,1}x_{i,2}x_{i,3}$ moving frame can be represented as,

$$ {}^{i}\mathbf{r}_{Q/O_i} = \underbrace{\eta_i\,{}^{i}\mathbf{x}_{i,1}}_{Rigid} + \underbrace{\sum_{j=1}^{m}\delta_{ij}(t)\mathbf{r}_{ij}(\eta)}_{Elastic} \tag{1}$$

where ${}^{i}\mathbf{x}_{i,1} = \{1 \quad 0 \quad 0\}^T$ and η_i is the distance between points Q and O_i when this link is assumed to be rigid. Also, $\mathbf{r}_{ij} = \{x_{1ij} \quad x_{2ij} \quad x_{3ij}\}^T$ is the eigen function vector which consists of longitudinal and bending mode shapes (x_{1ij}, x_{2ij} and x_{3ij}). Furthermore, the rotation of Q can be expressed by assumed mode method (AMM) as,

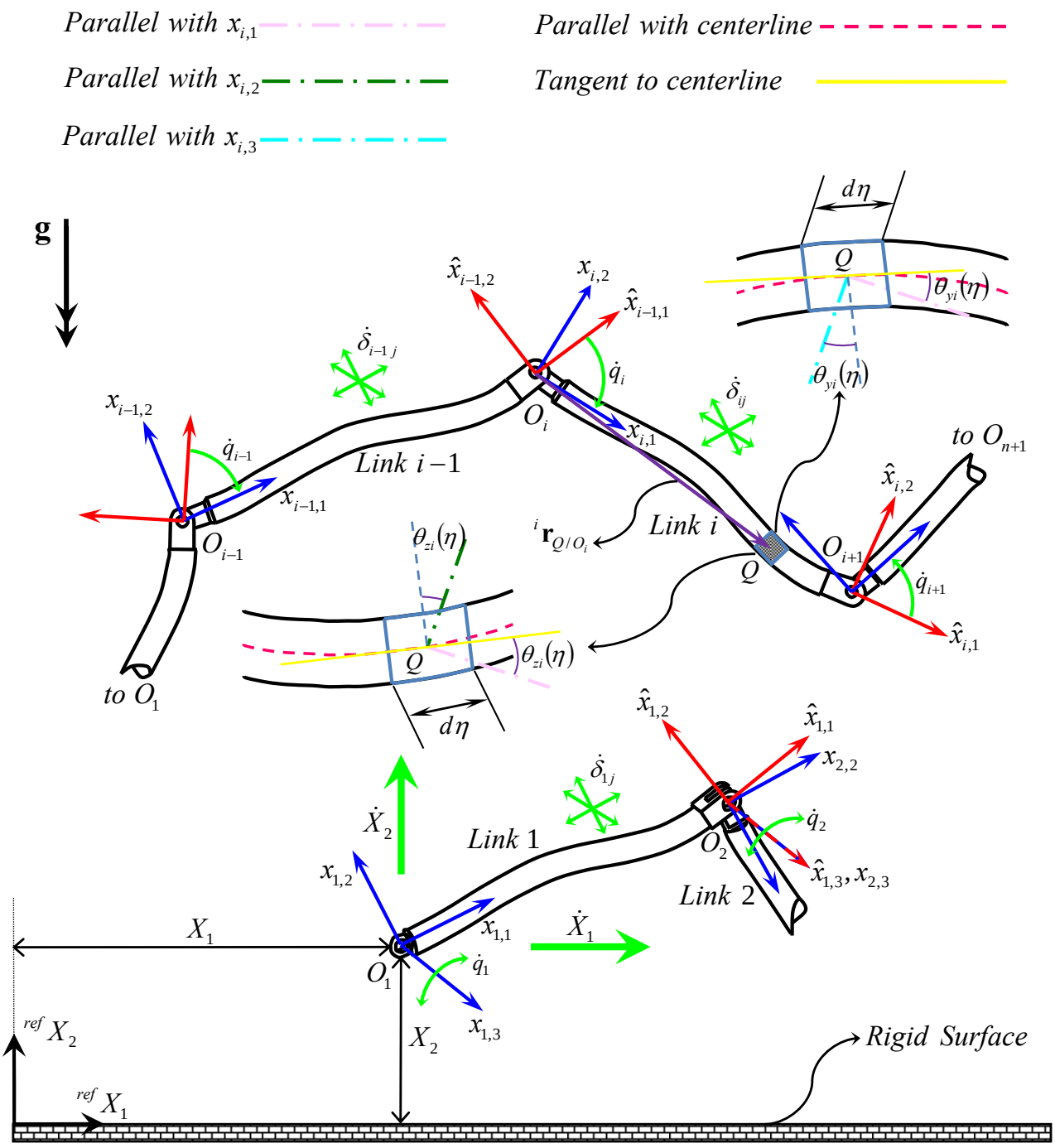

Fig. 1. A falling down multi-flexible links

$$ {}^i\boldsymbol{\theta}_i = \sum_{j=1}^{m} \delta_{ij}(t)\boldsymbol{\theta}_{ij}(\eta) \tag{2}$$

where $\boldsymbol{\theta}_{ij} = \left\{\theta_{x_1ij} \quad \theta_{x_2ij} \quad \theta_{x_3ij}\right\}^T$ is the eigen function vector which includes rotational shape functions (θ_{x_1ij}, θ_{x_2ij} and θ_{x_3ij}) in principle axes ($O_i x_{i,1}$, $O_i x_{i,2}$ and $O_i x_{i,3}$).

As the approach proposed in this paper is according to the G-A methodology, the absolute acceleration of Q is needed. This term can be expressed as,

$$ {}^i\ddot{\mathbf{r}}_Q = {}^i\ddot{\mathbf{r}}_{O_i} + {}^i\ddot{\mathbf{r}}_{Q/O_i} + 2{}^i\boldsymbol{\omega}_i \times {}^i\dot{\mathbf{r}}_{Q/O_i} + {}^i\dot{\boldsymbol{\omega}}_i \times {}^i\mathbf{r}_{Q/O_i} + {}^i\boldsymbol{\omega}_i \times \left({}^i\boldsymbol{\omega}_i \times {}^i\mathbf{r}_{Q/O_i}\right) \tag{3} $$

where ${}^i\ddot{\mathbf{r}}_{O_i}$ is the acceleration of the i^{th} joint and ${}^i\boldsymbol{\omega}_i$ is the angular velocity of the i^{th} link. Also, ${}^i\dot{\mathbf{r}}_{Q/O_i}$ and ${}^i\ddot{\mathbf{r}}_{Q/O_i}$ can be obtained by once and twice differentiating of Eq. (1), respectively. In following section, Eq. (3) will be employed to establish the Gibbs function (acceleration energy) of the system.

3. Dynamics of a falling down multi-flexible link

In this section, two dynamical models, namely, flying phase and impact phase are developed to study the dynamic behavior of multi-flexible-link robotic systems. The finite motion of the above-mentioned robotic system during the flying phase will be obtained by differential equations, while the impulsive motion due to the collision of this mechanical system with the ground will be formulated by algebraic equations. In below, the details of these two phases are described.

3.1. Dynamics of the system in the flying phase

In the flying phase, the manipulator is suspended through the space and has no contact with the ground [38]. In this paper, differential equations for the flying phase are attained by the G-A formulation, in which the acceleration energy and potential energy of each elastic link are calculated first, and then theses partial terms are added together for all flexible links to provide the Gibbs function (S) and the potential energy (V) of the whole system. Here, it should be noted that all dynamical methods lead to the same motion equations. However, the approach suggested in this study is based on the G-A formulation which involves with less computational counts.

3.1.1. Gibbs function of the whole system

The Acceleration energy of a serial robotic manipulator which consists of n flexible links with lengths l_i can be presented as,

$$ S = \sum_{i=1}^{n} \int_0^{l_i} \left[\frac{1}{2} \mu_i(\eta_i) \left({}^i\ddot{\mathbf{r}}_Q^T \cdot {}^i\ddot{\mathbf{r}}_Q \right) + \frac{1}{2} {}^i\dot{\boldsymbol{\omega}}_i^T \cdot J_i'(\eta_i)^i\dot{\boldsymbol{\omega}}_i \right] d\eta_i \tag{4} $$

where ${}^i\tilde{\omega}_i$ is the skew symmetric tensor associated with vector ${}^i\boldsymbol{\omega}_i$. By introducing Eq. (3) into Eq. (4) one may obtain:

$$S=\sum_{i=1}^{n}\frac{1}{2}B_{0i}\,{}^{i}\ddot{\mathbf{r}}_{O_i}^{T}\cdot{}^{i}\ddot{\mathbf{r}}_{O_i}+{}^{i}\ddot{\mathbf{r}}_{O_i}^{T}\cdot{}^{i}\mathbf{B}_{1i}-2^{i}\ddot{\mathbf{r}}_{O_i}^{T}\cdot B_{2i}\,{}^{i}\boldsymbol{\omega}_i-{}^{i}\ddot{\mathbf{r}}_{O_i}^{T}\cdot B_{3i}\,{}^{i}\dot{\boldsymbol{\omega}}_i-{}^{i}\ddot{\mathbf{r}}_{O_i}^{T}\cdot{}^{i}\tilde{\omega}_i B_{3i}\,{}^{i}\boldsymbol{\omega}_i$$
$$+\frac{1}{2}B_{4i}-2^{i}\boldsymbol{\omega}_i^{T}\cdot{}^{i}\mathbf{B}_{5i}+{}^{i}\dot{\boldsymbol{\omega}}_i^{T}\cdot{}^{i}\mathbf{B}_{6i}-{}^{i}\boldsymbol{\omega}_i^{T}\cdot B_{7i}\,{}^{i}\boldsymbol{\omega}_i+2^{i}\dot{\boldsymbol{\omega}}_i^{T}\cdot B_{8i}\,{}^{i}\boldsymbol{\omega}_i \tag{5}$$
$$+\frac{1}{2}{}^{i}\dot{\boldsymbol{\omega}}_i^{T}\cdot\left(B_{9i}+B_{10i}\right){}^{i}\dot{\boldsymbol{\omega}}_i+{}^{i}\dot{\boldsymbol{\omega}}_i^{T}\cdot{}^{i}\tilde{\omega}_i B_{9i}\,{}^{i}\boldsymbol{\omega}_i+\textit{irrelevant terms}$$

where

$$B_{0i}=\int_0^{l_i}\mu_i(\eta)d\eta \qquad {}^{i}\mathbf{B}_{1i}=\sum_{j=1}^{m}\ddot{\delta}_{ij}(t)\mathbf{C}_{1ij} \qquad B_{2i}=\sum_{j=1}^{m}\dot{\delta}_{ij}(t)\tilde{C}_{1ij}$$

$$B_{3i}=C_{2i}+\sum_{j=1}^{m}\delta_{ij}(t)\tilde{C}_{1ij} \qquad B_{4i}=\sum_{j=1}^{m}\sum_{k=1}^{m}\ddot{\delta}_{ij}(t)\ddot{\delta}_{ik}(t)C_{3ijk} \qquad {}^{i}\mathbf{B}_{5i}=\sum_{j=1}^{m}\sum_{k=1}^{m}\ddot{\delta}_{ij}(t)\dot{\delta}_{ik}(t)\mathbf{C}_{4ijk}$$

$${}^{i}\mathbf{B}_{6i}=\sum_{j=1}^{m}\ddot{\delta}_{ij}(t)\boldsymbol{\alpha}_{ij} \qquad B_{7i}=\sum_{j=1}^{m}\ddot{\delta}_{ij}(t)\beta_{ij} \qquad B_{8i}=\sum_{j=1}^{m}\dot{\delta}_{ij}(t)\beta_{ij} \tag{6-16}$$

$$B_{9i}=C_{5i}+\sum_{j=1}^{m}\delta_{ij}(t)\left(C_{6ij}^{T}+\beta_{ij}\right) \qquad B_{10i}=\int_0^{l_i}J_i'(\eta)d\eta$$

In the G-A method, the governing equations are derived by differentiating the acceleration energy with respect to quasi-accelerations (linear combination of generalized accelerations). Thus, it is not necessary to evaluate those terms in Gibbs function that do not encompass $\ddot{q}_j$, $\ddot{\delta}_{jf}$ and $\ddot{X}_j$ as quasi-accelerations. As observed in Eq. (5), all these terms are named as "irrelevant terms". Also all the variables appearing in Eqs. (6-16), including the integrations of mode shape products can be expressed as:

$$\mathbf{C}_{1ij}=\int_0^{l_i}\mu_i(\eta)\mathbf{r}_{ij}(\eta)d\eta \qquad C_{2i}=\int_0^{l_i}\mu_i(\eta)\eta\,{}^{i}\tilde{x}_{i,1}d\eta$$

$$C_{3ijk}=\int_0^{l_i}\mu_i(\eta)\mathbf{r}_{ij}^{T}(\eta)\cdot\mathbf{r}_{ik}(\eta)d\eta \qquad \mathbf{C}_{4ijk}=\int_0^{l_i}\mu_i(\eta)\tilde{r}_{ij}(\eta)\mathbf{r}_{ik}(\eta)d\eta$$

$$C_{5i}=\int_0^{l_i}\mu_i(\eta)\eta^{2}\,{}^{i}\tilde{x}_{i,1}^{T}\,{}^{i}\tilde{x}_{i,1}d\eta \qquad C_{6ij}=\int_0^{l_i}\mu_i(\eta)\eta\,{}^{i}\tilde{x}_{i,1}^{T}\tilde{r}_{ij}(\eta)d\eta \tag{17-26}$$

$$\mathbf{C}_{7ij}=\int_0^{l_i}\mu_i(\eta)\eta\,{}^{i}\tilde{x}_{i,1}\,\mathbf{r}_{ij}(\eta)d\eta \qquad C_{8ijk}=\int_0^{l_i}\mu_i(\eta)\tilde{r}_{ij}^{T}(\eta)\tilde{r}_{ik}(\eta)d\eta$$

$$\boldsymbol{\alpha}_{ij}=\mathbf{C}_{7ij}+\sum_{k=1}^{m}\delta_{ik}(t)\mathbf{C}_{4ikj} \qquad \beta_{ij}=C_{6ij}+\sum_{k=1}^{m}\delta_{ik}(t)C_{8ikj}$$

As mentioned above, one should evaluate the derivatives of acceleration energy with respect to quasi-accelerations. So, we get:

Differentiation with respect to $\ddot{q}_j$

$$\frac{\partial S}{\partial \ddot{q}_j}=\sum_{i=j+1}^{n}\frac{\partial^i \ddot{\mathbf{r}}_{O_i}^T}{\partial \ddot{q}_j}\cdot\left(B_{0i}{}^i\ddot{\mathbf{r}}_{O_i}+{}^i\mathbf{B}_{1i}-2B_{2i}{}^i\boldsymbol{\omega}_i-B_{3i}{}^i\dot{\boldsymbol{\omega}}_i-{}^i\tilde{\omega}_i B_{3i}{}^i\boldsymbol{\omega}_i\right)$$
$$+\sum_{i=j}^{n}\frac{\partial^i \dot{\boldsymbol{\omega}}_i^T}{\partial \ddot{q}_j}\cdot\left(B_{3i}{}^i\ddot{\mathbf{r}}_{O_i}+{}^i\mathbf{B}_{6i}+2B_{8i}{}^i\boldsymbol{\omega}_i+\left(B_{9i}+B_{10i}\right){}^i\dot{\boldsymbol{\omega}}_i+{}^i\tilde{\omega}_i B_{9i}{}^i\boldsymbol{\omega}_i\right) \tag{27}$$

$$j=1....\ n$$

Differentiation with respect to $\ddot{\delta}_{jf}$

$$\frac{\partial S}{\partial \ddot{\delta}_{jf}}=\sum_{i=j+1}^{n}\frac{\partial^i \ddot{\mathbf{r}}_{O_i}^T}{\partial \ddot{\delta}_{jf}}\cdot\left(B_{0i}{}^i\ddot{\mathbf{r}}_{O_i}+{}^i\mathbf{B}_{1i}-2B_{2i}{}^i\boldsymbol{\omega}_i-B_{3i}{}^i\dot{\boldsymbol{\omega}}_i-{}^i\tilde{\omega}_i B_{3i}{}^i\boldsymbol{\omega}_i\right)$$
$$+\sum_{i=j+1}^{n}\frac{\partial^i \dot{\boldsymbol{\omega}}_i^T}{\partial \ddot{\delta}_{jf}}\cdot\left(B_{3i}{}^i\ddot{\mathbf{r}}_{O_i}+{}^i\mathbf{B}_{6i}+2B_{8i}{}^i\boldsymbol{\omega}_i+\left(B_{9i}+B_{10i}\right){}^i\dot{\boldsymbol{\omega}}_i+{}^i\tilde{\omega}_i B_{9i}{}^i\boldsymbol{\omega}_i\right)$$
$$+\sum_{k=1}^{m}\ddot{\delta}_{jk}C_{3jfk}-2{}^j\boldsymbol{\omega}_j^T\cdot\sum_{k=1}^{m}\dot{\delta}_{jk}\mathbf{C}_{4jfk}-{}^j\boldsymbol{\omega}_j^T\cdot\beta_{jf}{}^j\boldsymbol{\omega}_j+{}^j\ddot{\mathbf{r}}_{O_j}^T\cdot\mathbf{C}_{1jf}+{}^j\dot{\boldsymbol{\omega}}_j^T\cdot\boldsymbol{\alpha}_{jf} \tag{28}$$

$$j=1.....\ n$$
$$f=1.....m$$

Differentiation with respect to $\ddot{X}_j$

$$\frac{\partial S}{\partial \ddot{X}_j}=\sum_{i=1}^{n}\frac{\partial^i \ddot{\mathbf{r}}_{O_i}^T}{\partial \ddot{X}_j}\cdot\left(B_{0i}{}^i\ddot{\mathbf{r}}_{O_i}+\mathbf{B}_{1i}-2B_{2i}{}^i\boldsymbol{\omega}_i-B_{3i}{}^i\dot{\boldsymbol{\omega}}_i-{}^i\tilde{\omega}_i B_{3i}{}^i\boldsymbol{\omega}_i\right) \tag{29}$$

$$j=1....\ 2$$

3.2.1. Potential energy of a falling down multi-flexible-link system

The potential energy of a falling down n-flexible-link robotic manipulator arises from two sources: 1) Gravity and 2) Strain energy. The effect of gravity can be considered by assuming that the origin of the global coordinate system has an acceleration of $1g$ to the top. However, to obtain the strain energy, one may refer to [32] where this function has been evaluated as,

$$V_e=\frac{1}{2}\sum_{i=1}^{n}\sum_{j=1}^{m}\sum_{k=1}^{m}\delta_{ij}(t)\delta_{ik}(t)K_{ijk} \tag{30}$$

in which

$$K_{ijk}=\int_0^{l_i}\left[G_iI_{x_1i}\frac{\partial\theta_{x_1ij}}{\partial\eta}\frac{\partial\theta_{x_1ik}}{\partial\eta}+E_iI_{x_2i}\frac{\partial\theta_{x_2ij}}{\partial\eta}\frac{\partial\theta_{x_2ik}}{\partial\eta}+E_iI_{x_3i}\frac{\partial\theta_{x_3ij}}{\partial\eta}\frac{\partial\theta_{x_3ik}}{\partial\eta}+E_iA_i\frac{\partial x_{1ij}}{\partial\eta}\frac{\partial x_{1ik}}{\partial\eta}\right]d\eta \quad (31)$$

where I_{x_ji} ($j=1,2,3$) are the area moments of inertia about the principle axes ($O_ix_{i,1}$, $O_ix_{i,2}$ and $O_ix_{i,3}$). Motion equations of the aforementioned robotic arm will be completed by taking the derivatives of potential energy with respect to the quasi-coordinates. So, we get:

Differentiation with respect to $\ddot{q}_j$

$$\frac{\partial V_e}{\partial q_j}=0 \qquad j=1....\ n \quad (32)$$

Differentiation with respect to $\ddot{\delta}_{jf}$

$$\frac{\partial V_e}{\partial \delta_{jf}}=\sum_{k=1}^{m}\delta_{jk}(t)K_{jkf} \qquad j=1.....\ n;\ \ f=1.....m \quad (33)$$

Differentiation with respect to $\ddot{X}_j$

$$\frac{\partial V_e}{\partial X_j}=0 \qquad j=1....\ 2 \quad (34)$$

3.1.2. Inverse dynamic equations of a falling down n-flexible-link robotic arm

Here, it is assumed there are no torque on the joints and no load on the links. With this proposition, the motion equations of the above-mentioned robotic system, in the flying phase, can be obtained as follows:

The rotational motion equations of the joins

$$\frac{\partial S}{\partial \ddot{q}_j}=0 \qquad j=1....\ n \quad (35)$$

The vibrational motion equations of the links

$$\frac{\partial S}{\partial \ddot{\delta}_{jf}}+\frac{\partial V_e}{\partial \delta_{jf}}=0 \qquad j=1.....\ n;\ \ f=1.....m \quad (36)$$

The translational motion equations of O_1

$$\frac{\partial S}{\partial \ddot{X}_j}=0 \qquad j=1....\ 2 \quad (37)$$

For the computer simulation of the aforementioned robotic system, the inverse dynamic form of the motion equations (Eqs. (35-37)) should be transformed to the direct dynamic form. The details are presented in the following section.

3.2. Direct dynamics of a falling down flexible multiple links

In this section, Eqs. (35-37) are converted to the following direct dynamics form:

$$I_f\left(\Theta\right)\ddot{\mathbf{\Theta}} = \mathbf{Re}\left(\Theta,\dot{\Theta}\right) \tag{38}$$

where $I_f\left(\Theta\right)$ is the inertia matrix of this n-elastic-link robotic system in the flying phase. Also $\ddot{\mathbf{\Theta}}$ and $\mathbf{Re}\left(\Theta,\dot{\Theta}\right)$ can be represented as

$$\ddot{\mathbf{\Theta}} = \left\{\ddot{q}_1 \quad \ddot{\delta}_{11} \quad ... \quad \ddot{\delta}_{1m} \quad \ddot{q}_2 \quad \ddot{\delta}_{21} \quad ... \quad \ddot{\delta}_{2m} \quad ... \quad \ddot{q}_n \quad \ddot{\delta}_{n1} \quad ... \quad \ddot{\delta}_{nm} \quad \ddot{X}_1 \quad \ddot{X}_2\right\}^T \tag{39}$$

$$\begin{aligned}\mathbf{Re}\left(\Theta,\dot{\Theta}\right) = \left\{\right.&\mathrm{Re}_{q_1} \quad \mathrm{Re}_{\delta_{11}} \quad ... \quad \mathrm{Re}_{\delta_{1m}} \quad \mathrm{Re}_{q_2} \quad \mathrm{Re}_{\delta_{21}} \quad ... \quad \mathrm{Re}_{\delta_{2m}} \\ &... \quad \mathrm{Re}_{q_n} \quad \mathrm{Re}_{\delta_{n1}} \quad ... \quad \mathrm{Re}_{\delta_{nm}} \quad \mathrm{Re}_{X_1} \quad \mathrm{Re}_{X_2}\left.\right\}^T\end{aligned} \tag{40}$$

In continue, the derivatives of ${}^i\ddot{\mathbf{r}}_{O_i}$ and ${}^i\dot{\boldsymbol{\omega}}_i$ with respect to $\ddot{q}_j$, $\ddot{\delta}_{jf}$ and $\ddot{X}_j$ appearing in Eqs. (27-29) should be computed. These two terms in summation form can be written as:

$${}^i\ddot{\mathbf{r}}_{O_i} = {}^i\ddot{\mathbf{r}}_{O_{s,i}} + {}^i\ddot{\mathbf{r}}_{O_{v,i}} \tag{41}$$

$${}^i\dot{\boldsymbol{\omega}}_i = {}^i\dot{\boldsymbol{\omega}}_{s,i} + {}^i\dot{\boldsymbol{\omega}}_{v,i} \tag{42}$$

where ${}^i\ddot{\mathbf{r}}_{O_{s,i}}$ and ${}^i\dot{\boldsymbol{\omega}}_{s,i}$ denote those parts of ${}^i\ddot{\mathbf{r}}_{O_i}$ and ${}^i\dot{\boldsymbol{\omega}}_i$ that encompass the generalized accelerations; while ${}^i\ddot{\mathbf{r}}_{O_{v,i}}$ and ${}^i\dot{\boldsymbol{\omega}}_{v,i}$ represent those parts of ${}^i\ddot{\mathbf{r}}_{O_i}$ and ${}^i\dot{\boldsymbol{\omega}}_i$ that do not include $\ddot{q}_j$, $\ddot{\delta}_{jf}$ and $\ddot{X}_j$ as generalized accelerations. These four terms can be presented as,

$${}^i\ddot{\mathbf{r}}_{O_{s,i}} = \sum_{j=1}^{2} {}^iR_{ref}\,{}^{ref}\mathbf{X}_j\ddot{X}_j + \sum_{k=1}^{i-1} {}^iR_k\left({}^k\ddot{\mathbf{r}}_{O_{k+1}/O_k} + {}^k\dot{\boldsymbol{\omega}}_{s,k}\times{}^k\mathbf{r}_{O_{k+1}/O_k}\right) \tag{43}$$

$${}^i\ddot{\mathbf{r}}_{O_{v,i}} = {}^iR_{ref}\,{}^{ref}\mathbf{X}_2 g + \sum_{k=1}^{i-1} {}^iR_k\left({}^k\boldsymbol{\omega}_k\times\left(2\,{}^k\dot{\mathbf{r}}_{O_{k+1}/O_k} + {}^k\boldsymbol{\omega}_k\times{}^k\mathbf{r}_{O_{k+1}/O_k}\right) + {}^k\dot{\boldsymbol{\omega}}_{v,k}\times{}^k\mathbf{r}_{O_{k+1}/O_k}\right) \tag{44}$$

$${}^i\dot{\boldsymbol{\omega}}_{s,i} = \sum_{k=1}^{i} {}^iR_k\,{}^k\mathbf{x}_{k,3}\ddot{q}_k + \sum_{k=1}^{i-1} {}^iR_k\,{}^k\ddot{\boldsymbol{\theta}}_k\left(l_k\right) \tag{45}$$

$${}^i\dot{\boldsymbol{\omega}}_{v,i} = \sum_{k=1}^{i-1} {}^iR_k\left({}^k\vec{\omega}_k + {}^k\dot{\boldsymbol{\theta}}_k\left(l_k\right)\right)\times{}^iR_{k+1}\,{}^{k+1}\mathbf{x}_{k+1,3}\,\dot{q}_{k+1} + \sum_{k=1}^{i-1} {}^iR_k\left({}^k\boldsymbol{\omega}_k\times{}^k\dot{\boldsymbol{\theta}}_k\left(l_k\right)\right) \tag{46}$$

where ${}^k\mathbf{r}_{O_{k+1}/O_k} = l_k\,{}^k\mathbf{x}_{k,1} + \sum_{j=1}^{m}\delta_{kj}\left(t\right)\mathbf{r}_{kj}\left(l_k\right)$, ${}^k\dot{\mathbf{r}}_{O_{k+1}/O_k}$ and ${}^k\ddot{\mathbf{r}}_{O_{k+1}/O_k}$ are obtained by differentiating of ${}^k\mathbf{r}_{O_{k+1}/O_k}$. Moreover, ${}^k\dot{\boldsymbol{\theta}}_k\left(l_k\right)$ and ${}^k\ddot{\boldsymbol{\theta}}_k\left(l_k\right)$ can be attained by time differentiations of Eq. (2).

Also, ${}^{ref}\mathbf{X}_1=\{1 \quad 0 \quad 0\}^T$, ${}^{ref}\mathbf{X}_2=\{0 \quad 1 \quad 0\}^T$, ${}^{ref}\mathbf{X}_3=\{0 \quad 0 \quad 1\}^T$ and ${}^{k}\mathbf{x}_{k,3}=\{0 \quad 0 \quad 1\}^T$. Finally, ${}^{i}R_k$ is a rotation matrix that indicates the orientation of the $x_{k,1}x_{k,2}x_{k,3}$ moving frame with respect to the $x_{i,1}x_{i,2}x_{i,3}$ one. For more details about ${}^{i}R_k$ one may refer to [30]. Now, the derivatives of ${}^{i}\ddot{\mathbf{r}}_{O_i}$ and ${}^{i}\dot{\boldsymbol{\omega}}_i$ with respect to $\ddot{q}_j$, $\ddot{\delta}_{jf}$ and $\ddot{X}_j$ can be written as,

$$\frac{\partial^i \ddot{\mathbf{r}}_{O_i}}{\partial \ddot{q}_j}={}^{i}R_j\,{}^{j}\mathbf{x}_{j,3}\times{}^{i}\mathbf{r}_{O_i/O_j} \qquad \frac{\partial^i \dot{\boldsymbol{\omega}}_i}{\partial \ddot{q}_j}={}^{i}R_j\,{}^{j}\mathbf{x}_{j,3} \tag{47-48}$$

$$\frac{\partial^i \ddot{\mathbf{r}}_{O_i}}{\partial \ddot{\delta}_{jf}}={}^{i}R_j\mathbf{r}_{jf}(l_j)+{}^{i}R_j\boldsymbol{\theta}_{jf}(l_j)\times{}^{i}\mathbf{r}_{O_i/O_{j+1}} \qquad \frac{\partial^i \dot{\boldsymbol{\omega}}_i}{\partial \ddot{\delta}_{jf}}={}^{i}R_j\boldsymbol{\theta}_{jf}(l_j) \tag{49-50}$$

$$\frac{\partial^i \ddot{\mathbf{r}}_{O_i}}{\partial \ddot{X}_j}={}^{i}R_{ref}\,{}^{ref}\mathbf{X}_j \tag{51}$$

3.2.1. Building the global inertia matrix and the global RHS vector

To establish the inertia matrix for this multi-flexible-link system in the flying phase, it is necessary to introduce Eqs. (43-46) and also Eqs. (47-51) into Eqs. (35-37). Then, all the expressions that contain generalized accelerations, i.e., $\ddot{q}_j$, $\ddot{\delta}_{jf}$ and $\ddot{X}_j$, should be kept on the left hand side (LHS) and all the remaining expressions should be taken to the RHS. By arranging the LHS expressions in a matrix format, the inertia matrix for this robotic system will be attained. The details of this procedure are explained below.

Generalized accelerations in the rotational differential equations: In Eq. (35), the expressions that encompass $\ddot{q}_k$, $\ddot{\delta}_{kt}$ and $\ddot{X}_k$ can be represented as,

$$\begin{aligned}
&\left[\sum_{k=1}^{n}\underbrace{{}^{j}\mathbf{x}_{j,3}^{T}\cdot{}^{j}\sigma_k\,{}^{k}\mathbf{x}_{k,3}}_{1}+\sum_{k=1}^{n}\underbrace{-{}^{j}\mathbf{x}_{j,3}^{T}\cdot{}^{j}\psi_k\,{}^{k}\mathbf{x}_{k,3}}_{2}+\sum_{k=1}^{n-1}\underbrace{-{}^{j}\mathbf{x}_{j,3}^{T}\cdot{}^{j}U_k\,{}^{k}\mathbf{x}_{k,3}}_{3}\right]\ddot{q}_k\\
&+\left[\sum_{k=1}^{n-1}\sum_{t=1}^{m}\underbrace{{}^{j}\mathbf{x}_{j,3}^{T}\cdot{}^{j}\sigma_{k^+}\boldsymbol{\theta}_{kt}}_{4}+\sum_{k=1}^{n-1}\sum_{t=1}^{m}\underbrace{-{}^{j}\mathbf{x}_{j,3}^{T}\cdot{}^{j}\psi_{k^+}\boldsymbol{\theta}_{kt}}_{5}+\sum_{k=1}^{n-1}\sum_{t=1}^{m}\underbrace{{}^{j}\mathbf{x}_{j,3}^{T}\cdot{}^{j}\xi_{k^+}\mathbf{r}_{kt}}_{6}+\sum_{k=1}^{n-1}\sum_{t=1}^{m}\underbrace{{}^{j}\mathbf{x}_{j,3}^{T}\cdot{}^{j}\gamma_k\,\mathbf{r}_{kt}}_{7}\right.\\
&\left.+\sum_{k=1}^{n-2}\sum_{t=1}^{m}\underbrace{-{}^{j}\mathbf{x}_{j,3}^{T}\cdot{}^{j}U_{k^+}\boldsymbol{\theta}_{kt}}_{8}+\sum_{k=j+1}^{n}\sum_{t=1}^{m}\underbrace{{}^{j}\mathbf{x}_{j,3}^{T}\cdot{}^{j}\tilde{r}_{O_k/O_j}\,{}^{j}R_k\mathbf{C}_{1kt}}_{9}+\sum_{k=j}^{n}\sum_{t=1}^{m}\underbrace{{}^{j}\mathbf{x}_{j,3}^{T}\cdot{}^{j}R_k\boldsymbol{\alpha}_{kt}}_{10}\right]\ddot{\delta}_{kt}\\
&+\left[\sum_{k=n+1}^{n+2}\underbrace{{}^{j}\mathbf{x}_{j,3}^{T}\cdot{}^{j}\xi_{ref}\,{}^{ref}\mathbf{X}_{k-n}}_{11}+\sum_{k=n+1}^{n+2}\underbrace{{}^{j}\mathbf{x}_{j,3}^{T}\cdot{}^{j}\gamma_{ref}\,{}^{ref}\mathbf{X}_{k-n}}_{12}\right]\ddot{X}_{k-n}
\end{aligned} \tag{I}$$

$I_q(\Theta)$		$k=1$				$k=2$				...	$k=n$				$k=n+1$	$k=n+2$
		$\ddot{q}_1$	$\ddot{\delta}_{11}$	...	$\ddot{\delta}_{1m}$	$\ddot{q}_2$	$\ddot{\delta}_{21}$	...	$\ddot{\delta}_{2m}$	...	$\ddot{q}_n$	$\ddot{\delta}_{n1}$	...	$\ddot{\delta}_{nm}$	$\ddot{X}_1$	$\ddot{X}_2$
$j=1$	$\ddot{q}_1$	1+2+3	4+5+6+7+8+10			1+2+3	4+5+6+7+8+9+10				1+2	9+10			11+12	11+12
$j=2$	$\ddot{q}_2$	1+2+3	4+5+6+7+8			1+2+3	4+5+6+7+8+10				1+2	9+10			11+12	11+12
⋮	⋮															
$j=n$	$\ddot{q}_n$	1+3	4+6+8			1+3	4+6+8				1	10			11	11

Fig. 2. Inertia matrix of the rotational motion equations in the flight phase

where ${}^{j}\sigma_k$, ${}^{j}\psi_k$, ${}^{j}U_k$, ${}^{j}\sigma_{k^+}$, ${}^{j}\psi_{k^+}$, ${}^{j}U_{k^+}$, ${}^{j}\xi_{k^+}$, ${}^{j}\gamma_k$, ${}^{j}\xi_{ref}$ and ${}^{j}\gamma_{ref}$ are presented in Appendix. The constituent terms of Exp. (I), numbered from (1) to (12), form the inertia matrix of the rotational differential equations that illustrated in Fig. 2.

Coriolis and centrifugal forces in the rotational differential equations: In Eq. (35), if all the expressions that do not encompass generalized accelerations ($\ddot{q}_k$, $\ddot{\delta}_{kt}$ and $\ddot{X}_k$) are transferred to the RHS, one may obtain:

$$\mathrm{Re}_{q_j} = \underbrace{\sum_{i=j+1}^{n} -\frac{\partial^i \ddot{\mathbf{r}}_{O_i}^T}{\partial \ddot{q}_j} \cdot {}^i\mathbf{S}_i}_{13} + \underbrace{\sum_{i=j}^{n} -\frac{\partial^i \dot{\boldsymbol{\omega}}_i^T}{\partial \ddot{q}_j} \cdot {}^i\mathbf{T}_i}_{14} \tag{52}$$

where

$${}^i\mathbf{S}_i = B_{0i}\,{}^i\ddot{\mathbf{r}}_{O_{v,i}} - 2B_{2i}\,{}^i\boldsymbol{\omega}_i - B_{3i}\,{}^i\dot{\boldsymbol{\omega}}_{v,i} - {}^i\tilde{\omega}_i B_{3i}\,{}^i\boldsymbol{\omega}_i \tag{53}$$

$${}^i\mathbf{T}_i = B_{3i}\,{}^i\ddot{\mathbf{r}}_{O_{v,i}} + 2B_{8i}\,{}^i\boldsymbol{\omega}_i + \left(B_{9i} + B_{10i}\right){}^i\dot{\boldsymbol{\omega}}_{v,i} + {}^i\tilde{\omega}_i B_{9i}\,{}^i\boldsymbol{\omega}_i \tag{54}$$

The constituent terms of Eq. (52), numbered (13) and (14), construct the RHS vector of the rotational differential equations that depicted in Fig. 3.

Generalized accelerations in the vibrational differential equations: In Eq. (36), all the expressions that encompass generalized accelerations ($\ddot{q}_k$, $\ddot{\delta}_{kt}$ and $\ddot{X}_k$) as their coefficients can be represented as,

$$\vec{\mathrm{Re}}_q\left(\Theta,\dot{\Theta}\right) = \begin{array}{|c|c|c|c|c|c|c|} \hline \mathrm{Re}_{q_1} & \mathrm{Re}_{q_2} & \cdots & \mathrm{Re}_{q_j} & \cdots & \mathrm{Re}_{q_{n-1}} & \mathrm{Re}_{q_n} \\ \hline 13+14 & 13+14 & \cdots & 13+14 & \cdots & 13+14 & 14 \\ \hline \end{array}^T$$

Fig. 3. Right hand side of the rotational motion equations for the flight phase

$$
\begin{aligned}
&\Bigg[\underbrace{\sum_{k=1}^{n}\boldsymbol{\theta}_{jf}^{T}\cdot^{j^{+}}\sigma_{k}{}^{k}\vec{x}_{k,3}}_{15}+\underbrace{\sum_{k=1}^{n}-\boldsymbol{\theta}_{jf}^{T}\cdot^{j^{+}}\psi_{k}{}^{k}\mathbf{x}_{k,3}}_{16}+\underbrace{\sum_{k=1}^{n-1}-\boldsymbol{\theta}_{jf}^{T}\cdot^{j^{+}}U_{k}{}^{k}\mathbf{x}_{k,3}}_{17}+\underbrace{\sum_{k=1}^{n}-\mathbf{r}_{jf}^{T}\cdot^{j^{+}}\xi_{k}{}^{k}\mathbf{x}_{k,3}}_{18}\\
&+\underbrace{\sum_{k=1}^{n-1}-\mathbf{r}_{jf}^{T}\cdot^{j}V_{k}{}^{k}\mathbf{x}_{k,3}}_{19}+\underbrace{\sum_{k=1}^{j-1}-\mathbf{C}_{1jf}^{T}\cdot^{j}W_{k}{}^{k}\mathbf{x}_{k,3}}_{20}+\underbrace{\sum_{k=1}^{j}\boldsymbol{\alpha}_{jf}^{T}\cdot^{j}R_{k}{}^{k}\mathbf{x}_{k,3}}_{21}\Bigg]\ddot{q}_{k}+\Bigg[\underbrace{\sum_{k=1}^{n-1}\sum_{t=1}^{m}\boldsymbol{\theta}_{jf}^{T}\cdot^{j^{+}}\sigma_{k^{+}}\boldsymbol{\theta}_{kt}}_{22}\\
&+\underbrace{\sum_{k=1}^{n-1}\sum_{t=1}^{m}-\boldsymbol{\theta}_{jf}^{T}\cdot^{j^{+}}\psi_{k^{+}}\boldsymbol{\theta}_{kt}}_{23}+\underbrace{\sum_{k=1}^{n-2}\sum_{t=1}^{m}-\boldsymbol{\theta}_{jf}^{T}\cdot^{j^{+}}U_{k^{+}}\boldsymbol{\theta}_{kt}}_{24}+\underbrace{\sum_{k=1}^{n-2}\sum_{t=1}^{m}-\mathbf{r}_{jf}^{T}\cdot^{j}V_{k^{+}}\boldsymbol{\theta}_{kt}}_{25}+\underbrace{\sum_{k=1}^{n-1}\sum_{t=1}^{m}-\mathbf{r}_{jf}^{T}\cdot^{j^{+}}\xi_{k^{+}}\boldsymbol{\theta}_{kt}}_{26}\\
&+\underbrace{\sum_{k=1}^{j-2}\sum_{t=1}^{m}-\mathbf{C}_{1jf}^{T}\cdot^{j}W_{k^{+}}\boldsymbol{\theta}_{kt}}_{27}+\underbrace{\sum_{k=1}^{j-1}\sum_{t=1}^{m}\boldsymbol{\alpha}_{jf}^{T}\cdot^{j}R_{k}\boldsymbol{\theta}_{kt}}_{28}+\underbrace{\sum_{t=1}^{m}C_{3jft}}_{29}+\underbrace{\sum_{k=1}^{n-1}\sum_{t=1}^{m}\boldsymbol{\theta}_{jf}^{T}\cdot^{j^{+}}\gamma_{k}\,\mathbf{r}_{kt}}_{30}+\underbrace{\sum_{k=1}^{n-1}\sum_{t=1}^{m}\boldsymbol{\theta}_{jf}^{T}\cdot^{j^{+}}\xi_{k^{+}}\,\mathbf{r}_{kt}}_{31}\qquad\text{(II)}\\
&+\underbrace{\sum_{k=1}^{n-1}\sum_{t=1}^{m}\mathbf{r}_{jf}^{T}\cdot^{j}\lambda_{k}\mathbf{r}_{kt}}_{32}+\underbrace{\sum_{k=1}^{j-1}\sum_{t=1}^{m}\mathbf{C}_{1jf}^{T}\cdot^{j}R_{k}\mathbf{r}_{kt}}_{33}+\underbrace{\sum_{k=j+1}^{n}\sum_{t=1}^{m}\mathbf{r}_{jf}^{T}\cdot^{j}R_{k}\mathbf{C}_{1kt}}_{34}+\underbrace{\sum_{k=j+2}^{n}\sum_{t=1}^{m}\boldsymbol{\theta}_{jf}^{T}\cdot^{j}\tilde{r}_{O_{k}/O_{j+1}}{}^{j}R_{k}\mathbf{C}_{1kt}}_{35}\\
&+\underbrace{\sum_{k=j+1}^{n}\sum_{t=1}^{m}\boldsymbol{\theta}_{jf}^{T}\cdot^{j}R_{k}\boldsymbol{\alpha}_{kt}}_{36}\Bigg]\ddot{\delta}_{kt}+\Bigg[\underbrace{\sum_{k=n+1}^{n+2}\mathbf{r}_{jf}^{T}\cdot^{j}\lambda_{ref}{}^{ref}\mathbf{X}_{k-n}}_{37}+\underbrace{\sum_{k=n+1}^{n+2}\boldsymbol{\theta}_{jf}^{T}\cdot^{j^{+}}\gamma_{ref}{}^{ref}\mathbf{X}_{k-n}}_{38}\\
&+\underbrace{\sum_{k=n+1}^{n+2}\boldsymbol{\theta}_{jf}^{T}\cdot^{j^{+}}\xi_{ref}{}^{ref}\mathbf{X}_{k-n}}_{39}+\underbrace{\sum_{k=n+1}^{n+2}\mathbf{C}_{1jf}^{T}\cdot^{j}R_{ref}{}^{ref}\mathbf{X}_{k-n}}_{40}\Bigg]\ddot{X}_{k-n}
\end{aligned}
$$

The constituent terms of Exp. (II), numbered from (15) to (40), establish the inertia matrix of the vibrational differential equations as illustrated in Fig. 4.

$I_{\delta}(\Theta)$		$k=1$				$k=2$				...	$k=n$				$k=n+1$	$k=n+2$
		$\ddot{q}_1$	$\ddot{\delta}_{11}$	...	$\ddot{\delta}_{1m}$	$\ddot{q}_2$	$\ddot{\delta}_{21}$	...	$\ddot{\delta}_{2m}$	...	$\ddot{q}_n$	$\ddot{\delta}_{n1}$	...	$\ddot{\delta}_{nm}$	$\ddot{X}_1$	$\ddot{X}_2$
$j=1$	$\ddot{\delta}_{11}$ ⋮ $\ddot{\delta}_{1m}$	15 +16 +17 +18 +19 +21	22+23+24+25+26 29+30+31+32			15 +16 +17 +18 +19	22+23+24+25+26 +30+31+32+34+36				15 +16 +18	34+35+36			37+38 39+40	37+38 39+40
$j=2$	$\ddot{\delta}_{21}$ ⋮ $\ddot{\delta}_{2m}$	15 +16 +17 +18 +19 +20 +21	22+23+24+25+26 28+30+31+32+33			15 +16 +17 +18 +19 +21	22+23+24+25+26 29+30+31+32				15 +16 +18	34+35+36			37+38 39+40	37+38 39+40
⋮	⋮															
$j=n$	$\ddot{\delta}_{n1}$ ⋮ $\ddot{\delta}_{nm}$	20 +21	27+28+33			20 +21	27+28+33				21	29			40	40

Fig. 4. Inertia matrix of the vibrational motion equations for the flight phase

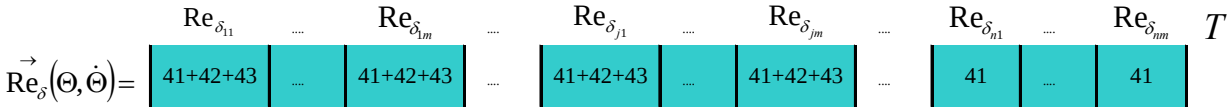

Fig. 5. Right hand side of the vibrational motion equations for the flight phase

Coriolis and centrifugal forces in the vibrational differential equations: In Eq. (36), all the expressions that do not encompass the quasi-accelerations can be presented as,

$$\mathrm{Re}_{\delta_{jf}} = \underbrace{Q_{jf}}_{41} + \underbrace{\sum_{i=j+1}^{n} -\frac{\partial^i \ddot{\mathbf{r}}_{O_i}^T}{\partial \ddot{\delta}_{jf}} \cdot {}^i\mathbf{S}_i}_{42} + \underbrace{\sum_{i=j+1}^{n} -\frac{\partial^i \dot{\boldsymbol{\omega}}_i^T}{\partial \ddot{\delta}_{jf}} \cdot {}^i\mathbf{T}_i}_{43} \tag{55}$$

where

$$Q_{jf} = -\sum_{k=1}^{m} \delta_{jk} K_{jkf} + 2\,{}^j\boldsymbol{\omega}_j^T \cdot \sum_{k=1}^{m} \dot{\delta}_{jk} \mathbf{C}_{4\,jfk} + {}^j\boldsymbol{\omega}_j^T \cdot \beta_{jf}\, {}^j\boldsymbol{\omega}_j - {}^j\ddot{\mathbf{r}}_{O_{v,j}}^T \cdot \mathbf{C}_{1\,jf} - {}^j\dot{\boldsymbol{\omega}}_{v,j}^T \cdot \boldsymbol{\alpha}_{jf} \tag{56}$$

The constituent terms of Eq. (55), which are numbered from (41) to (43), form the RHS vector of the vibrational differential equations as demonstrated in Fig. 5.

Generalized accelerations in the translational differential equations: In Eq. (37), all the expressions that encompass $\ddot{q}_k$, $\ddot{\delta}_{kt}$ and $\ddot{X}_k$ have been gathered as,

$$\begin{aligned}
&\left[\sum_{k=1}^{n-1} \underbrace{-{}^{ref}\mathbf{X}_{j-n}^T \cdot {}^{ref}V_k\, {}^k\mathbf{x}_{k,3}}_{44} + \sum_{k=1}^{n} \underbrace{-{}^{ref}\mathbf{X}_{j-n}^T \cdot {}^{ref}\xi_k\, {}^k\mathbf{x}_{k,3}}_{45}\right]\ddot{q}_k + \left[\sum_{k=1}^{n-1}\sum_{t=1}^{m} \underbrace{{}^{ref}\mathbf{X}_{j-n}^T \cdot {}^{ref}\lambda_k \mathbf{r}_{kt}}_{46}\right. \\
&\left. + \sum_{k=1}^{n}\sum_{t=1}^{m} \underbrace{{}^{ref}\mathbf{X}_{j-n}^T \cdot {}^{ref}R_k \mathbf{C}_{1kt}}_{47} + \sum_{k=1}^{n-2}\sum_{t=1}^{m} \underbrace{-{}^{ref}\mathbf{X}_{j-n}^T \cdot {}^{ref}V_{k^+} \boldsymbol{\theta}_{kt}}_{48} + \sum_{k=1}^{n-1}\sum_{t=1}^{m} \underbrace{-{}^{ref}\mathbf{X}_{j-n}^T \cdot {}^{ref}\xi_{k^+} \boldsymbol{\theta}_{kt}}_{49}\right]\ddot{\delta}_{kt} + \underbrace{M_{tot}}_{50}\ddot{X}_{j-n}
\end{aligned} \tag{III}$$

where ${}^{ref}V_k$, ${}^{ref}\lambda_k$, ${}^{ref}\xi_k$, ${}^{ref}V_{k^+}$, ${}^{ref}\xi_{k^+}$ and M_{tot} are presented in the Appendix. The constituent terms of Exp. (III), which are numbered from (44) to (50), form the inertia matrix of the translational differential equations as displayed in Fig. 6.

$I_X(\Theta)$		$k=1$				$k=2$				...	$k=n$				$k=n+1$	$k=n+2$
		$\ddot{q}_1$	$\ddot{\delta}_{11}$	...	$\ddot{\delta}_{1m}$	$\ddot{q}_2$	$\ddot{\delta}_{21}$	...	$\ddot{\delta}_{2m}$	...	$\ddot{q}_n$	$\ddot{\delta}_{n1}$	...	$\ddot{\delta}_{nm}$	$\ddot{X}_1$	$\ddot{X}_2$
$j=n+1$	$\ddot{X}_1$	44 +45	46+47+48+49			44 +45	46+47+48+49				45	47			50	0
$j=n+2$	$\ddot{X}_2$	44 +45	46+47+48+49			44 +45	46+47+48+49				45	47			0	50

Fig. 6. Inertia matrix of the translational motion equations in the flight phase

$$\vec{\mathrm{Re}}_X(\Theta,\dot{\Theta}) = \begin{array}{|c|c|}\hline \mathrm{Re}_{X_1} & \mathrm{Re}_{X_2} \\ \hline 51 & 51 \\ \hline \end{array}^T$$

Fig. 7. Right hand side of the translational motion equations for the flight phase

Coriolis and centrifugal forces in the translational differential equations: In Eq. (37), all the expressions which do not encompass $\ddot{q}_k$, $\ddot{\delta}_{kt}$ and $\ddot{X}_k$ can be represented as:

$$\mathrm{Re}_{X_j} = \underbrace{\sum_{i=1}^{n} -\frac{\partial^i \ddot{\mathbf{r}}_{O_i}^T}{\partial \ddot{X}_j} \cdot {}^i\mathbf{S}_i}_{51} \tag{57}$$

The constructive term of Eq. (57) which is numbered (51), form the RHS vector of the translational differential equations as exhibited in Fig. 7.

3.2.2. Assembling the inertia matrices and the RHS vectors of motion equations

In the previous section, the inertia matrices for the rotational (Fig. 2), vibrational (Fig. 4) and translational (Fig. 6) motion equations were obtained. By assembling these three matrices, the inertia matrix of the system obtains as shown in Fig. 8.

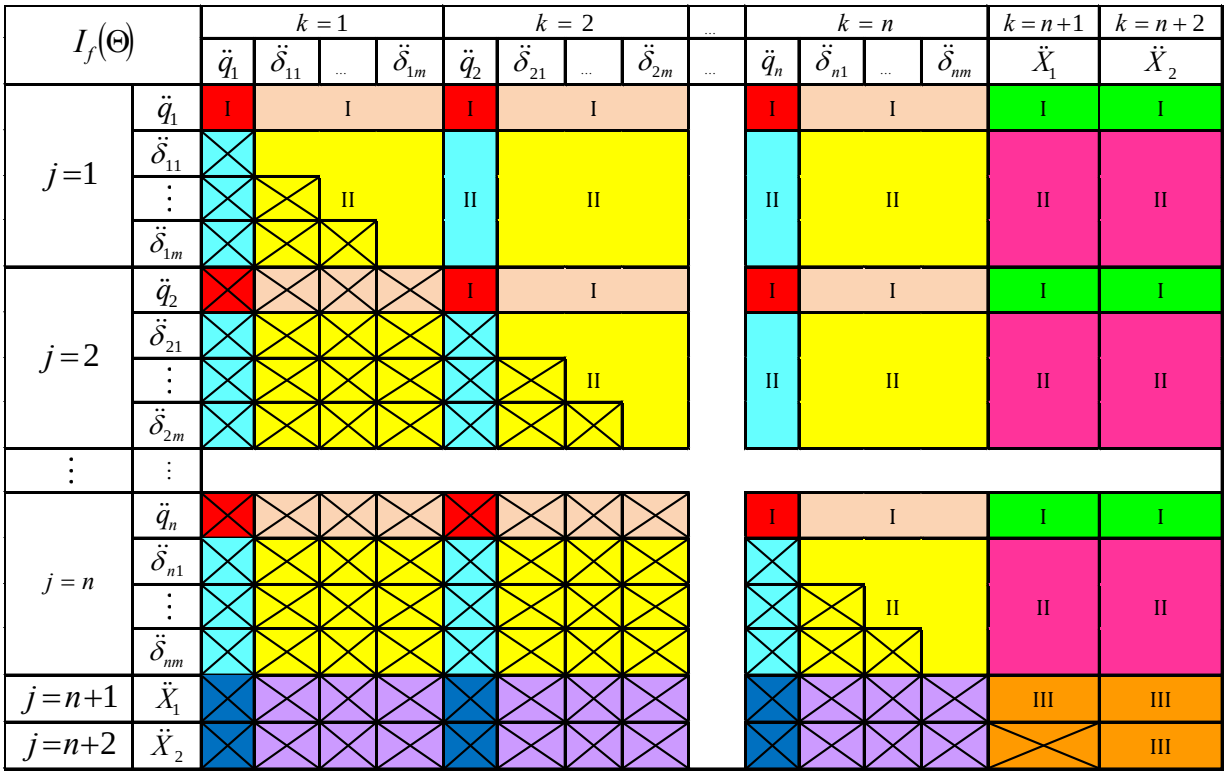

Fig. 8. Inertia matrix of the whole system in the flight phase

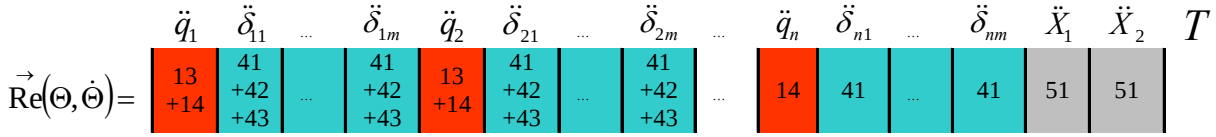

Fig. 9. Right hand side vector of governing equations for the flight phase

The inertia matrix of this robotic system is symmetric. Therefore, in Fig. 8, it is sufficient to compute only those parts that are specified as (I), (II) and (III). This procedure is covered with details in the Appendix. Finally, by assembling the RHS vectors in the rotational (Fig. 3), vibrational (Fig. 5) and translational (Fig. 7) differential equations, Coriolis and centrifugal forces of the motion equations in the flight phase will be obtained as shown in Fig. 9.

3.3. Dynamics of the system in the impact phase

To accomplish the objectives of this section, the absolute velocity of each joint should be determined first. Apparently, for a serial manipulator constructed of n elastic links, there are $n+1$ joints and end points. The absolute velocities of these $n+1$ points can be represented as,

$$^{ref}\dot{\mathbf{r}}_{O_i}\left(\Theta,\dot{\Theta}\right)=J\left(\Theta\right)\dot{\Theta} \tag{58}$$

where $J(\Theta)$ is the Jacobian matrix of the aforementioned robotic system which is illustrated in Fig. 10. It should be noted that $\partial^{ref}\mathbf{r}_{O_i}/\partial\Theta_j$ is the derivative of the i^{th} joint's position with respect to the j^{th} generalized coordinate. Also $^{i}J_{j,:}$ represents the Jacobian matrix for the j^{th} row ($j=1....3$) and every column ($1....n+2$) of the i^{th} joint ($i=1....n+1$).

An impact phenomenon happens when any joint or end point of the above-mentioned robotic system touches the ground. So, by considering Eq. (38), the system's motion equations in the impact phase can be presented as,

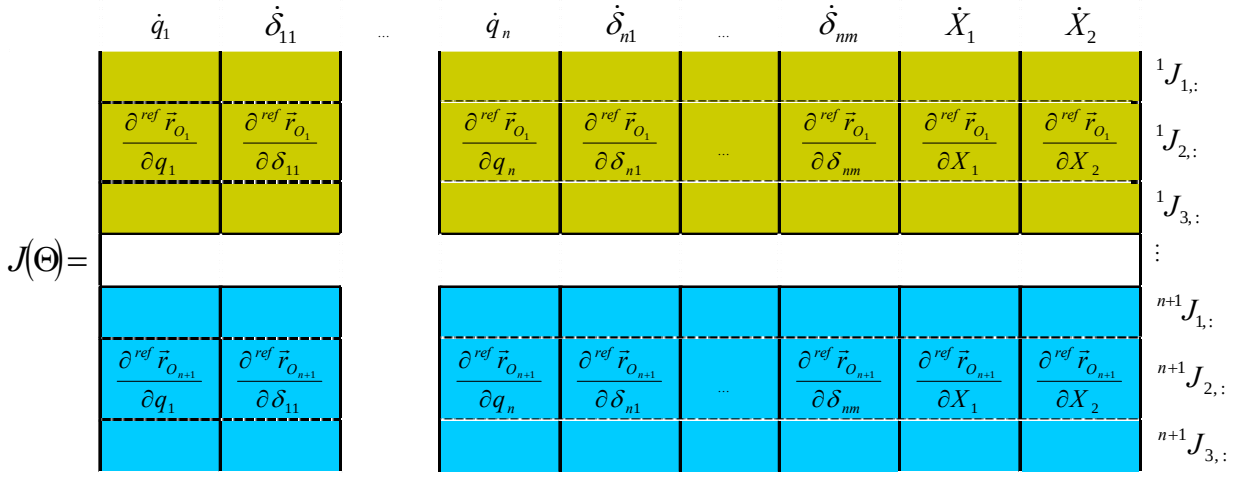

Fig. 10. Jacobian matrix of n flying flexible links

$$I_f(\Theta)\ddot{\boldsymbol{\Theta}} = \mathbf{Re}(\Theta,\dot{\Theta}) + J^T(\Theta)\delta\mathbf{F}(t) \tag{59}$$

where $\delta\mathbf{F}(t)$ indicates the applied forces exerting on the joints or end points during their collisions with the ground. By integrating Eq. (59) over the impact time ($t^- \to t^+$), we get:

$$I_f(\Theta^-)(\dot{\boldsymbol{\Theta}}^+ - \dot{\boldsymbol{\Theta}}^-) = J^T(\Theta^-)\mathbf{F} \quad \Rightarrow \quad \left[I_f(\Theta^-)\middle| -J^T(\Theta^-)\right]\begin{Bmatrix}\dot{\boldsymbol{\Theta}}^+\\ \mathbf{F}\end{Bmatrix} = \left[I_f(\Theta^-)\right]\{\dot{\boldsymbol{\Theta}}^-\} \tag{60}$$

where $\mathbf{F} = \int_{t^-}^{t^+} \delta\mathbf{F}(t)dt$ and also, $\dot{\boldsymbol{\Theta}}^-$ / $\dot{\boldsymbol{\Theta}}^+$ are the generalized velocities just before/after an impact. Eq. (60) presents *n+nm+2* equations and *n+nm+2+Number of Contact Points* unknowns. The additional equations can be obtained by having the relationship between the pre- and post-impact velocities of joints or end points that collide with the ground, as follows:

$$J(\Theta^-)\dot{\boldsymbol{\Theta}}^+ = -eJ(\Theta^-)\dot{\boldsymbol{\Theta}}^- \tag{61}$$

In above equation, which is called the Newton's impact law, e denotes the coefficient of restitution. By combining Eqs. (60) and (61) and forming them in matrix format, we get

$$\underbrace{\left[\begin{array}{c|c} I_f(\Theta^-) & -J^T(\Theta^-) \\ \hline J(\Theta^-) & 0 \end{array}\right]}_{I_i}\begin{Bmatrix}\dot{\boldsymbol{\Theta}}^+\\ \mathbf{F}\end{Bmatrix} = \begin{bmatrix} I_f(\Theta^-) \\ -eJ(\Theta^-)\end{bmatrix}\{\dot{\boldsymbol{\Theta}}^-\} \tag{62}$$

For example, if two impulsive forces of $\delta F_p^{X_2}(t)$ and $\delta F_q^{X_1}(t)$ are respectively and simultaneously exerted on the p^{th} joint in the ${}^{ref}\mathbf{X}_2$ direction and on the q^{th} joint in the ${}^{ref}\mathbf{X}_1$ direction, then two rows and columns should be incorporated to the initial inertia matrix obtained for the flying phase to establish the inertia matrix in the impact phase (see Fig. 11). Pre-multiplication of both sides in Eq. (62) by $I_i^{-1}(\Theta)$ provides the unknown variables. The outcomes of the impact phase are the new initial conditions for the next flying phase.

4. Computer simulations

Here, the results of two computer simulations are presented to verify the proposed model.

Case study 1*:* For the first simulation, a planar single flexible link which is shown in Fig. 12, is simulated. This system is released with the following initial conditions.

$$\begin{aligned} &q_1\big|_{t=0} = 0\,rad;\ \delta_{11}\big|_{t=0} = 0;\ X_1\big|_{t=0} = 0m;\ X_2\big|_{t=0} = 0.5m;\\ &\dot{q}_1\big|_{t=0} = 0\frac{rad}{s};\ \dot{\delta}_{11}\big|_{t=0} = 0\frac{1}{s};\ \dot{X}_1 = \dot{X}_2\big|_{t=0} = 0\frac{m}{s};\end{aligned} \tag{63}$$

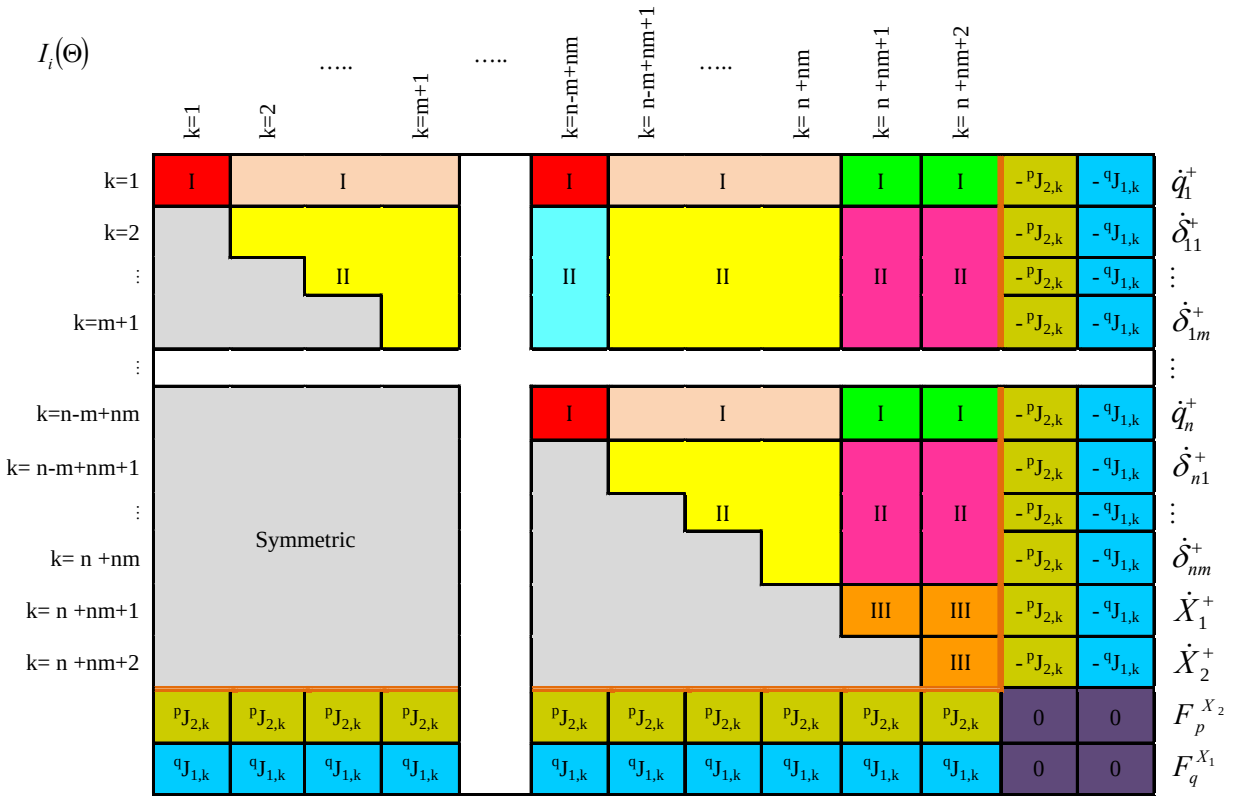

Fig. 11. A sample inertia matrix of the impact phase

The elastic properties of this flexible link is modeled by the first eigen function of EBBT with clamped-clamped boundary conditions.

$$x_{211} = \sin(4.731\eta) - 1.017\cos(4.731\eta) - \sinh(4.731\eta) + 1.017\cosh(4.731\eta) \tag{63}$$

$$\theta_{x_3 11} = \frac{dx_{211}}{d\eta} \tag{64}$$

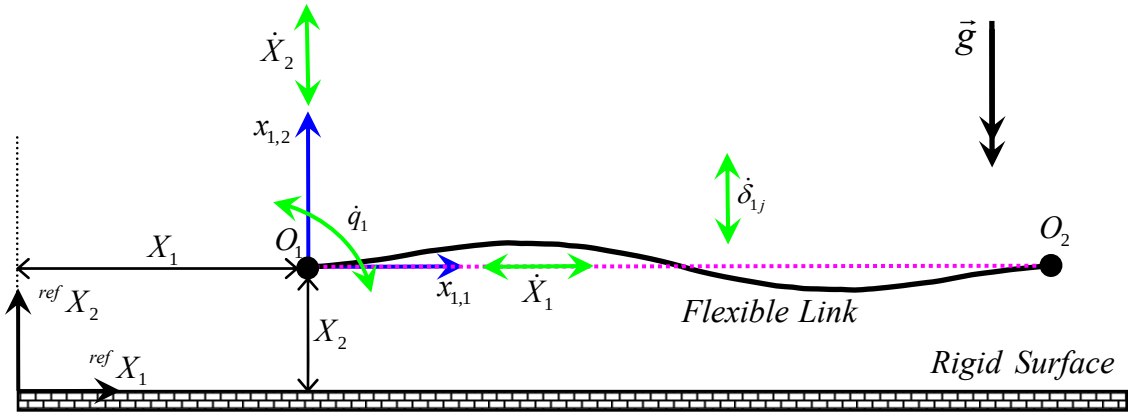

Fig. 12. A single flexible link released from a specific height

Table 1. Required parameters for simulating the planar motion of a single flexible flying link

Parameters	**Value**	**Unit**
Length of the link	$l_1 = 1$	m
Mass per unit length	$\mu_1 = 1$	$\mathrm{kg \cdot m^{-1}}$
Bending stiffness	$EI_{x_3} = 1000$	$\mathrm{N \cdot m^2}$
Mass moment of inertia per unit length	$J_1 = \begin{bmatrix} 5.89 & 0 & 0 \\ 0 & 2.94 & 0 \\ 0 & 0 & 2.94 \end{bmatrix} \times 10^{-5}$	$\mathrm{kg \cdot m}$
Gravity	$g = 9.81$	$\mathrm{m \cdot s^{-2}}$
Coefficient of restitution	$e = 1$	

The necessary parameters for the simulation can be found in Table 1. Also, the results of the numerical solutions are depicted in Figs. 13-20.

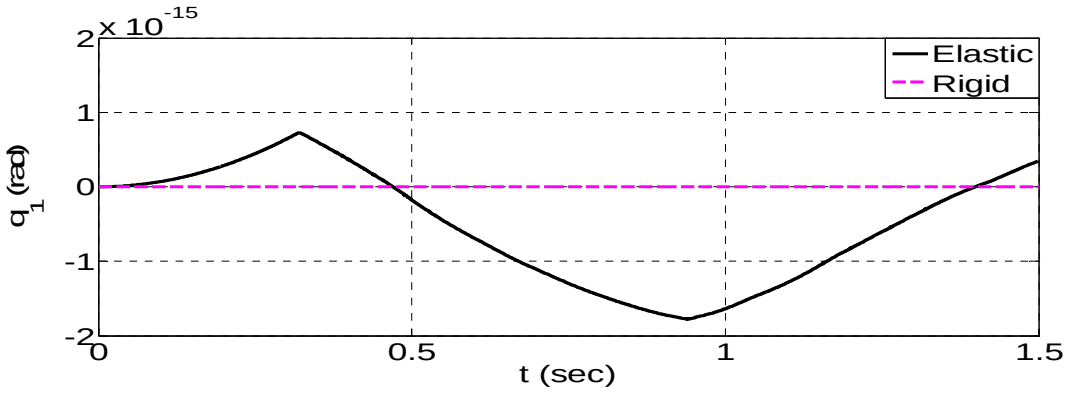

Fig. 13. Angular position of the flexible link

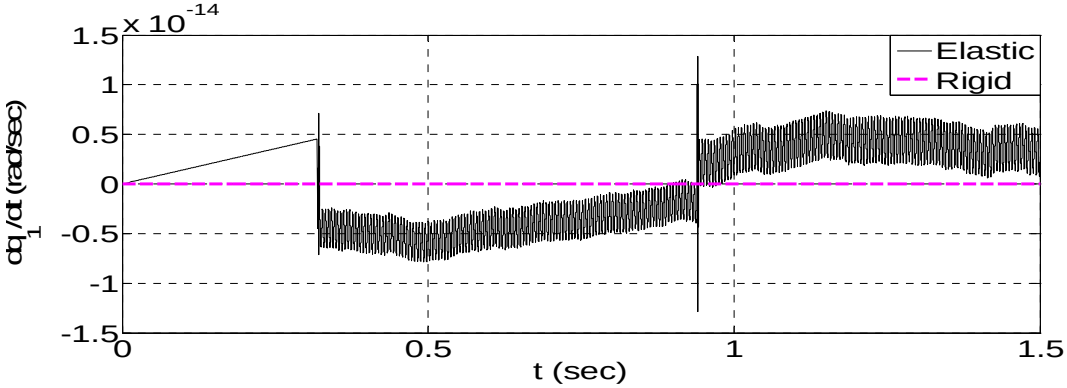

Fig. 14. Angular velocity of the flexible link

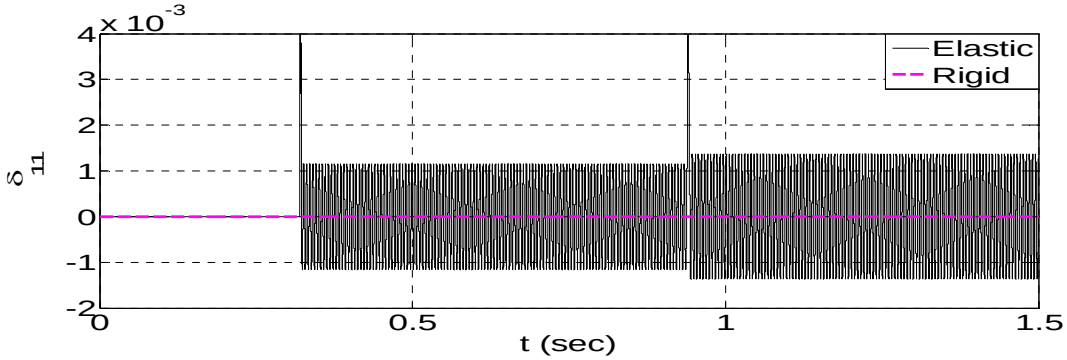

Fig. 15. Flexural displacement of the flexible link

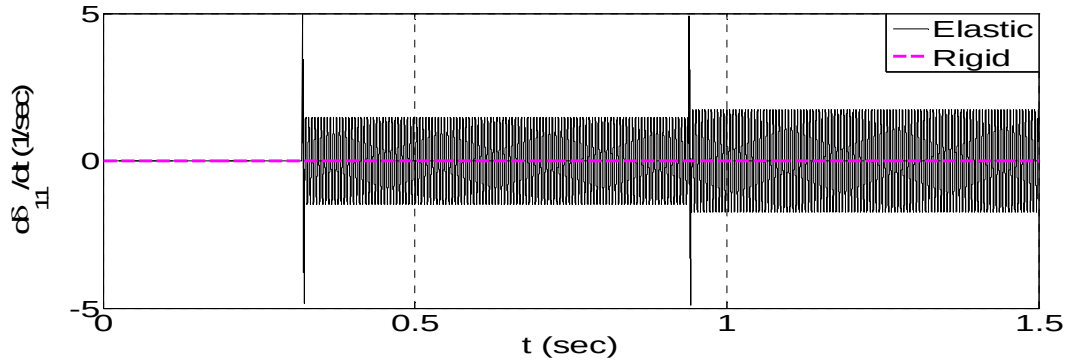

Fig. 16. Modal generalized velocity of the flexible link

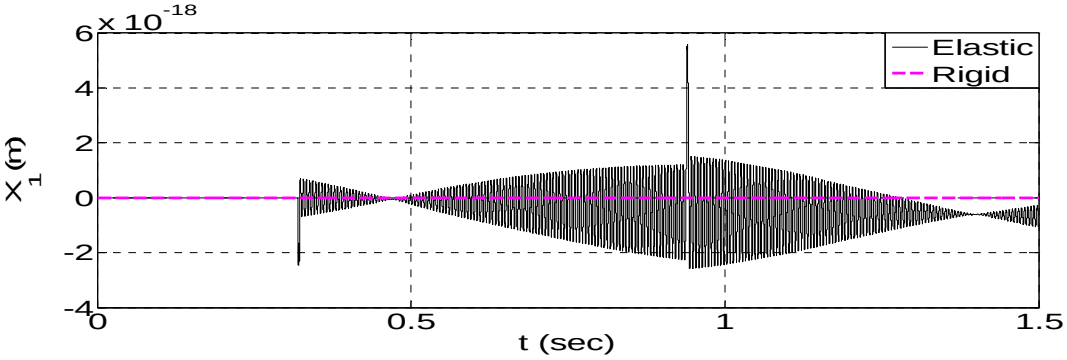

Fig. 17. Horizontal position of O_1

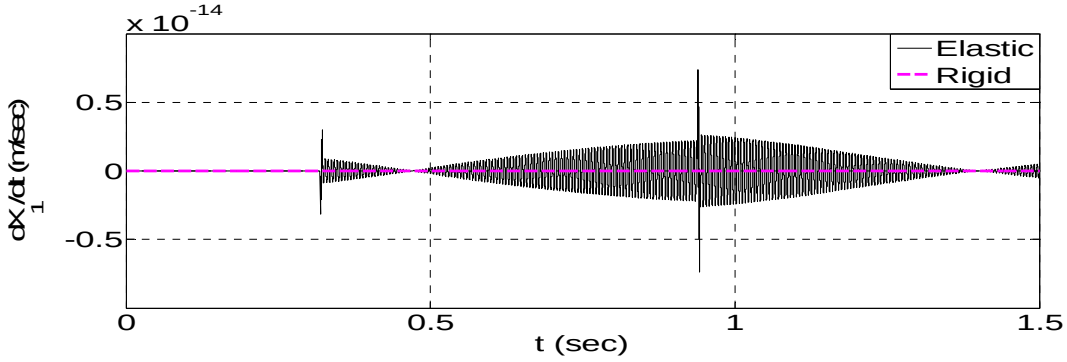

Fig. 18. Absolute velocity of O_1 in the $^{ref}X_1$ direction

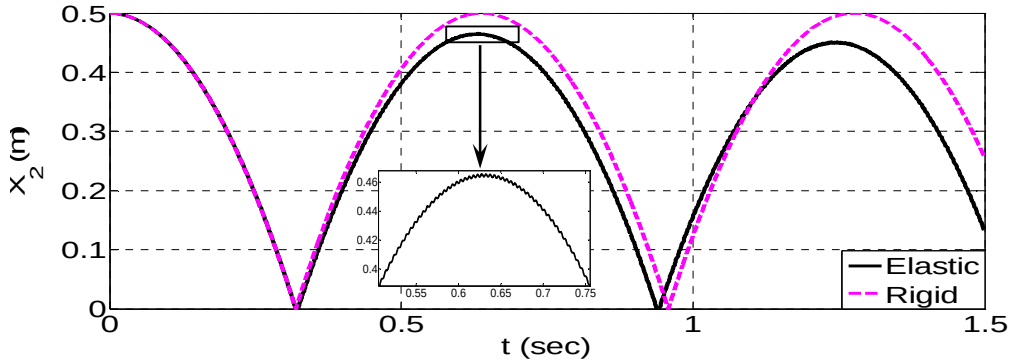

Fig. 19. Vertical position of O_1

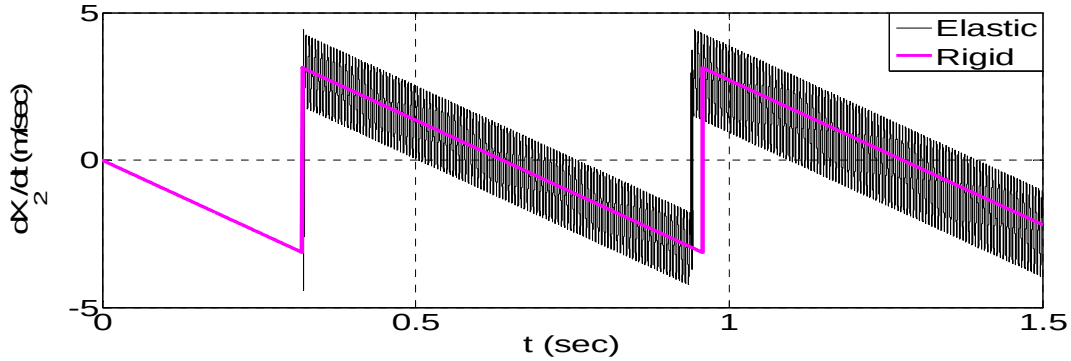

Fig. 20. Absolute velocity of O_1 in the $^{ref}X_2$ direction

The simulation results indicate that the system collides with the rigid surface at two different times: $t = 0.3194\,\text{sec}$ and $t = 0.9388\ \text{sec}$. The flexible link has almost no rotational motion. This fact can be concluded from Fig. 13 and Fig. 14. Also, the horizontal motion of this elastic link is negligible according to Fig. 17 and Fig. 18. Fig. 19 indicates that when the link is assumed rigid, it will reach its initial height ($X_2 = 0.5m$), based on the conservation of energy law. When the link is assumed flexible, it will not reach its initial position. This is predictable; because when the elastic link strikes the ground, part of its energy will be converted to vibration energy due to the excitation of vibrational modes.

***Case study 2**:* The purpose of the second case study is to compare the computational complexity of the algorithm proposed in the current paper with the method presented in [37]. A two-flexible-link planar robotic manipulator confined within a circle is simulated for this purpose. The computer simulation results of this model can be found in Figs. 12-20 of [37]. As expected, the same results are obtained by the developed algorithm proposed in the current work. To save space, the time responses of this system have not been presented in the current paper. However, the computational procedures required to obtain the governing equations of the aforementioned robotic systems by both recursive algorithms are presented in Table 2. In general, the required number of mathematical operations of 3×3 rotational matrices is less than that of 4×4 transformation matrices. For example, the CPU time for deriving the motion equations of this two-link flexible robotic system taken by the Intel (R) Core (TM) i3-3220 processor running at 3.3 GHz is 17.96 sec for the 3×3 rotational matrices and 21.13 sec for the 4×4 transformation matrices respectively.

Table 2: Required mathematical operations for recursive algorithms based on 3×3 rotational matrices and 4×4 transformation matrices

Sums	Products	Method
$-18+26n-6m+13mn^2-4mn$ $+11m^2n^2-15m^2n+3m^2+5n^2$	$-27+\frac{75}{2}n-9m+18mn^2-6mn$ $+\frac{33}{2}m^2n^2-\frac{45}{2}m^2n+3m^2+\frac{9}{2}n^2$	3×3
$-33+48n-10m+25mn^2-9mn$ $+20m^2n^2-28m^2n+6m^2+4n^2$	$-41+\frac{125}{2}n-13m+27mn^2-10mn$ $+\frac{55}{2}m^2n^2-\frac{75}{2}m^2n+6m^2+\frac{15}{2}n^2$	4×4

Sums	Products	n=10; m=2
7062	9972	3×3
12551	16032	4×4

5. Conclusion

In this article, an automatic algorithm has been proposed for the mathematical modeling of finite and impulsive motions of n-elastic-link robotic systems with flying platform. Since the derivation of motion equations of this robotic arm is too complex, the developed procedure in this paper has been explained, graphically. As we know, when the D.O.F of the system increases, the Lagrangian formulation requires more total and partial differentiations relative to the Gibbs-Appell formulation. So, to accomplish the purpose of this paper, the governing equations in the flying phase are derived by exploiting the Gibbs-Appell formulation in recursive form. Moreover, to formulate the impulsive motion of the system, the application of Newton's kinematic impact law has been employed. More importantly, as is demonstrated in the manuscript, deriving the motion equations of the aforementioned robotic system by 3×3 rotational matrices instead of 4×4 transformation matrices can significantly improve the efficiency of the applied algorithm. Consequently, a less costly computational procedure can be used to satisfactorily simulate the same model.

Algorithms based on 3×3 rotational matrices enjoy unique benefits such as less computational steps; however, these algorithms suffer from lengthy formulations. Further research can thus focus on the development of an algorithm that combines 3×3 rotational matrices with 4×4 transformation matrices to strike a balance between high computational load and lengthy complicated formulations.

Appendix

The expressions appearing in the inertia matrix are defined as follows:

$${}^{j}\sigma_k=\sum_{i=\max(k,j)}^{n}{}^{j}R_i\left(B_{9i}+B_{10i}\right)^{i}R_k \qquad {}^{j}\sigma_{k^+}=\sum_{i=\max(k+1,j)}^{n}{}^{j}R_i\left(B_{9i}+B_{10i}\right)^{i}R_k \qquad {}^{j^+}\sigma_k=\sum_{i=\max(k,j+1)}^{n}{}^{j}R_i\left(B_{9i}+B_{10i}\right)^{i}R_k$$

$$ {}^{j^+}\sigma_{k^+} = \sum_{i=\max(k+1,j+1)}^{n} {}^{j}R_i\left(B_{9i}+B_{10i}\right){}^{i}R_k \qquad {}^{j}\psi_k = \sum_{i=\max(k,j+1)}^{n} {}^{j}\tilde{r}_{O_i/O_j}\,{}^{j}R_i B_{3i}\,{}^{i}R_k \qquad {}^{j}\psi_{k^+} = \sum_{i=\max(k+1,j+1)}^{n} {}^{j}\tilde{r}_{O_i/O_j}\,{}^{j}R_i B_{3i}\,{}^{i}R_k $$

$$ {}^{j^+}\psi_k = \sum_{i=\max(k,j+2)}^{n} {}^{j}\tilde{r}_{O_i/O_{j+1}}\,{}^{j}R_i B_{3i}\,{}^{i}R_k \qquad {}^{j^+}\psi_{k^+} = \sum_{i=\max(k+1,j+2)}^{n} {}^{j}\tilde{r}_{O_i/O_{j+1}}\,{}^{j}R_i B_{3i}\,{}^{i}R_k \qquad {}^{j}U_k = \sum_{t=k}^{n-1}\left({}^{j}\gamma_t + {}^{j}\xi_{t^+}\right){}^{t}\tilde{r}_{O_{t+1}/O_t}\,{}^{t}R_k $$

$$ {}^{j}U_{k^+} = \sum_{t=k+1}^{n-1}\left({}^{j}\gamma_t + {}^{j}\xi_{t^+}\right){}^{t}\tilde{r}_{O_{t+1}/O_t}\,{}^{t}R_k \qquad {}^{j^+}U_k = \sum_{t=k}^{n-1}\left({}^{j^+}\gamma_t + {}^{j^+}\xi_{t^+}\right){}^{t}\tilde{r}_{O_{t+1}/O_t}\,{}^{t}R_k \qquad {}^{j^+}U_{k^+} = \sum_{t=k+1}^{n-1}\left({}^{j^+}\gamma_t + {}^{j^+}\xi_{t^+}\right){}^{t}\tilde{r}_{O_{t+1}/O_t}\,{}^{t}R_k $$

$$ {}^{j}\xi_{k^+} = \sum_{i=\max(k+1,j)}^{n} {}^{j}R_i B_{3i}\,{}^{i}R_k \qquad {}^{j^+}\xi_k = \sum_{i=\max(k,j+1)}^{n} {}^{j}R_i B_{3i}\,{}^{i}R_k \qquad {}^{j^+}\xi_{k^+} = \sum_{i=\max(k+1,j+1)}^{n} {}^{j}R_i B_{3i}\,{}^{i}R_k $$

$$ {}^{j}\xi_{ref} = \sum_{i=j}^{n} {}^{j}R_i B_{3i}\,{}^{i}R_{ref} \qquad {}^{ref}\xi_k = \sum_{i=k}^{n} {}^{ref}R_i B_{3i}\,{}^{i}R_k \qquad {}^{j^+}\xi_{ref} = \sum_{i=j+1}^{n} {}^{j}R_i B_{3i}\,{}^{i}R_{ref} $$

$$ {}^{ref}\xi_{k^+} = \sum_{i=k+1}^{n} {}^{ref}R_i B_{3i}\,{}^{i}R_k \qquad {}^{j}\gamma_k = \sum_{i=\max(k+1,j+1)}^{n} {}^{j}\tilde{r}_{O_i/O_j} B_{0i}\,{}^{j}R_k \qquad {}^{j^+}\gamma_k = \sum_{i=\max(k+1,j+2)}^{n} {}^{j}\tilde{r}_{O_i/O_{j+1}} B_{0i}\,{}^{j}R_k $$

$$ {}^{j}\gamma_{ref} = \sum_{i=j+1}^{n} {}^{j}\tilde{r}_{O_i/O_j} B_{0i}\,{}^{j}R_{ref} \qquad {}^{j^+}\gamma_{ref} = \sum_{i=j+2}^{n} {}^{j}\tilde{r}_{O_i/O_{j+1}} B_{0i}\,{}^{j}R_{ref} \qquad {}^{j}V_k = \sum_{t=k}^{n-1} {}^{j}\lambda_t\,{}^{t}\tilde{r}_{O_{t+1}/O_t}\,{}^{t}R_k $$

$$ {}^{j}V_{k^+} = \sum_{t=k+1}^{n-1} {}^{j}\lambda_t\,{}^{t}\tilde{r}_{O_{t+1}/O_t}\,{}^{t}R_k \qquad {}^{ref}V_k = \sum_{t=k}^{n-1} {}^{ref}\lambda_t\,{}^{t}\tilde{r}_{O_{t+1}/O_t}\,{}^{t}R_k \qquad {}^{ref}V_{k^+} = \sum_{t=k+1}^{n-1} {}^{ref}\lambda_t\,{}^{t}\tilde{r}_{O_{t+1}/O_t}\,{}^{t}R_k $$

$$ {}^{j}W_k = \sum_{t=k}^{j-1} {}^{j}R_t\,{}^{t}\tilde{r}_{O_{t+1}/O_t}\,{}^{t}R_k \qquad {}^{j}W_{k^+} = \sum_{t=k+1}^{j-1} {}^{j}R_t\,{}^{t}\tilde{r}_{O_{t+1}/O_t}\,{}^{t}R_k \qquad {}^{j}\lambda_k = \sum_{i=\max(k+1,j+1)}^{n} B_{0i}\,{}^{j}R_k $$

$$ {}^{j}\lambda_{ref} = \sum_{i=j+1}^{n} B_{0i}\,{}^{j}R_{ref} \qquad {}^{ref}\lambda_k = \sum_{i=k+1}^{n} B_{0i}\,{}^{ref}R_k \qquad M_{tot} = \sum_{i=1}^{n} B_{0i} $$

(A.1) - (A.33)

Also, the inertia matrix of the whole system (Fig. 8) is constructed as follows:

Calculation of the inertia matrix for $\ddot{q}_k$ in the rotational motion equations (I):

$for\ \ j=1:n-1;\ k=j:n-1\ \Rightarrow\ I_{jk00}=1+2+3;$

$for\ \ j=1:n-1;\ k=n\ \Rightarrow\ I_{jk00}=1+2;$

$for\ \ j=n;\ k=n\ \Rightarrow\ I_{jk00}=1;$

Calculation of the inertia matrix for $\ddot{\delta}_{kt}$ in the rotational motion equations (I):

$for\ \ j=1:n-2;\ k=j;\ t=1:m\ \Rightarrow\ I_{jk0t}=4+5+6+7+8+10;$

$for\ \ j=1:n-3;\ k=j+1:n-2;\ t=1:m\ \ \Rightarrow\ I_{jk0t}=4+5+6+7+8+9+10;$

$for\ \ j=1:n-2;\ k=n-1;\ t=1:m\ \ \Rightarrow\ I_{jk0t}=4+5+6+7+9+10;$

$for\ \ j=n-1;\ k=n-1;\ t=1:m\ \ \Rightarrow\ I_{jk0t}=4+5+6+7+10;$

$for\ \ j=1:n-1;\ k=n;\ t=1:m\ \ \Rightarrow\ I_{jk0t}=9+10;$

$for\ \ j=n;\ k=n;\ t=1:m\ \ \Rightarrow\ I_{jk0t}=10;$

Calculation of the inertia matrix for $\ddot{X}_k$ in the rotational motion equations (I):

$for\ \ j=1:n-1;\ k=n+1:n+2\ \ \Rightarrow\ I_{jk00}=11+12;$

$for\ \ j=n;\ k=n+1:n+2\ \ \Rightarrow\ I_{jk00}=11;$

Calculation of the inertia matrix for $\ddot{q}_k$ in the vibrational motion equations (II):

$for\ \ j=1:n-2;\ k=j;\ f=1:m\ \ \Rightarrow\ I_{jkf0}=15+16+17+18+19+21;$

$for\ \ j=n-1;\ k=j;\ f=1:m\ \ \Rightarrow\ I_{jkf0}=15+17+18+19+21;$

$for\ \ j=1:n-2;\ k=j+1:n-1;\ f=1:m\ \ \Rightarrow\ I_{jkf0}=15+16+17+18+19;$

$for\ \ j=1:n-2;\ k=n;\ f=1:m\ \ \Rightarrow\ I_{jkf0}=15+16+18;$

$for\ \ j=n-1;\ k=n;\ f=1:m\ \ \Rightarrow\ I_{jkf0}=15+18;$

$for\ \ j=n;\ k=n;\ f=1:m\ \ \Rightarrow\ I_{jkf0}=21;$

Calculation of the inertia matrix for $\ddot{\delta}_{kt}$ in the vibrational motion equations (II):

$for\ \ j=1:n-2;\ k=j;\ f=1:m;\ t=1:m\ \ \Rightarrow\ I_{jkft}=22+23+24+25+26+29+30+31+32;$

$for\ \ j=1:n-3;\ k=j+1;\ f=1:m;\ t=1:m\ \ \Rightarrow\ I_{jkft}=22+23+24+25+26+30+31+32+34+36;$

$for\ \ j=1:n-4;\ k=j+2:n-2;\ f=1:m;\ t=1:m\ \ \Rightarrow\ I_{jkft}=22+23+24+25+26+30+31+32+34+35+36;$

$for\ \ j=1:n-3;\ k=n-1;\ f=1:m;\ t=1:m\ \ \Rightarrow\ I_{jkft}=22+23+26+30+31+32+34+35+36;$

$for\ \ j=n-2;\ k=n-1;\ f=1:m;\ t=1:m\ \ \Rightarrow\ I_{jkft}=22+23+26+30+31+32+34+36;$

$for\ \ j=n-1;\ k=n-1;\ f=1:m;\ t=1:m\ \ \Rightarrow\ I_{jkft}=22+26+29+31+32;$

$for\ \ j=1:n-2;\ k=n;\ f=1:m;\ t=1:m\ \ \Rightarrow\ I_{jkft}=34+35+36;$

$for\ \ j=n-1;\ k=n;\ f=1:m;\ t=1:m\ \ \Rightarrow\ I_{jkft}=34+36;$

$for\ \ j=n;\ k=n;\ f=1:m;\ t=1:m\ \ \Rightarrow\ I_{jkft}=29;$

Calculation of the inertia matrix for $\ddot{X}_k$ in the vibrational motion equations (II):

$$for \;\; j = 1:n-2;\; k = n+1:n+2; \;\; \Rightarrow \;\; I_{jk00} = 37+38+39+40;$$

$$for \;\; j = n-1;\; k = n+1:n+2; \;\; \Rightarrow \;\; I_{jk00} = 37+39+40;$$

$$for \;\; j = n;\; k = n+1:n+2; \;\; \Rightarrow \;\; I_{jk00} = 40;$$

Calculation of the inertia matrix for $\ddot{X}_k$ in the translational motion equations (III):

$$for \;\; j = n+1:n+2;\; k = j; \;\; \Rightarrow \;\; I_{jk00} = 50;$$

References

[1] J. Wittenburg, Dynamics of systems of rigid bodies, Vieweg+Teubner Verlag, 1977.
[2] C.C. Chang, S.T. Peng, Impulsive motion of multibody systems, Multibody System Dynamics, 17 (2007) 47-70.
[3] Y. Hurmuzlu, D.B. Marghitu, Rigid body collisions of planar kinematic chains with multiple contact points, The International Journal of Robotics Research, 13 (1994) 82-92.
[4] A. Rodriguez, A. Bowling, Solution to indeterminate multipoint impact with frictional contact using constraints, Multibody System Dynamics, 28 (2012) 313-330.
[5] M. Mahmoodi, M. Kojouri Manesh, M. Eghtesad, M. Farid, S. Movahed, Adaptive passivity-based control of a flexible-joint robot manipulator subject to collision, Proceedings of the Institution of Mechanical Engineers, Part C: Journal of Mechanical Engineering Science, 228 (2014) 840-849.
[6] C. Glocker, Energetic consistency conditions for standard impacts, Multibody System Dynamics, 29 (2013) 77-117.
[7] A. Tornambè, Modeling and control of impact in mechanical systems: Theory and experimental results, IEEE Transactions on Automatic Control, 44 (1999) 294-309.
[8] S. Liu, L. Wu, Z. Lu, Impact dynamics and control of a flexible dual-arm space robot capturing an object, Applied Mathematics and Computation, 185 (2007) 1149-1159.
[9] S.A. Modarres Najafabadi, J. Kövecses, J. Angeles, Energy analysis and decoupling in three-dimensional impacts of multibody systems, ASME Journal of Applied Mechanics, 74 (2007) 845-851.
[10] M. Hajiaghamemar, M. Seidi, J.R. Ferguson, V. Caccese, Measurement of head impact due to standing fall in adults using anthropomorphic test dummies, Annals of Biomedical Engineering, 43 (2015) 2143-2152.
[11] Z. Kariž, G.R. Heppler, A controller for an impacted single flexible link, Journal of Vibration and Control, 6 (2000) 407-428.
[12] D. Boghiu, D.B. Marghitu, The control of an impacting flexible link using fuzzy logic strategy, Journal of Vibration and Control, 4 (1998) 325-341.
[13] Y.A. Khulief, A.A. Shabana, A continuous force model for the impact analysis of flexible multibody systems, Mechanism and Machine Theory, 22 (1987) 213-224.
[14] A.S. Yigit, A.G. Ulsoy, R.A. Scott, Dynamics of a radially rotating beam with impact, Part 1: Theoretical and computational model, Journal of Vibration and Acoustics, 112 (1990) 65-70.
[15] A.S. Yigit, A.G. Ulsoy, R.A. Scott, Spring-dashpot models for the dynamics of a radially rotating beam with impact, Journal of Sound and Vibration, 142 (1990) 515-525.
[16] B.V. Chapnik, G.R. Heppler, J.D. Aplevich, Modeling impact on a one-link flexible robotic arm, IEEE Transactions on Robotics and Automation, 7 (1991) 479-488.
[17] Y.A. Khulief, Modeling of impact in multibody systems: An overview, Journal of Computational and Nonlinear Dynamics, 8 (2013) 1-15.
[18] Q. Yu, I.M. Chen, A general approach to the dynamics of nonholonomic mobile manipulator systems, ASME Journal of Dynamic Systems, Measurement and Control, 124 (2002) 512-521.
[19] Q. Sun, M. Nahon, I. Sharf, An inverse dynamics algorithm for multiple flexible-link manipulators, Journal of Vibration and Control, 6 (2000) 557-569.
[20] A. Mohan, S.K. Saha, A recursive, numerically stable, and efficient simulation algorithm for serial robots with flexible links, Multibody System Dynamics, 21 (2009) 1-35.

[21] U. Lugris, M.A. Naya, A. Luaces, J. Cuadrado, Efficient calculation of the inertia terms in floating frame of reference formulations for flexible multibody dynamics, Proceedings of the Institution of Mechanical Engineers, Part K: Journal of Multi-body Dynamics, 223 (2009) 147-157.
[22] U. Lugris, M.A. Naya, F. Gonzalez, J. Cuadrado, Performance and application criteria of two fast formulations for flexible multibody dynamics, Mechanics Based Design of Structures and Machines, 35 (2007) 381-404.
[23] Y.L. Hwang, Recursive Newton-Euler formulation for flexible dynamic manufacturing analysis of open-loop robotic systems, Int J Adv Manuf Technol, 29 (2006) 598-604.
[24] D.S. Bae, E.J. Haug, A recursive formulation for constrained mechanical system dynamics: Part I. Open loop systems, Journal of Structural Mechanics, 15 (1987) 359-382.
[25] T.M. Wasfy, A.K. Noor, Computational strategies for flexible multibody systems, Applied Mechanics Reviews, 56 (2003) 553-613.
[26] M.H. Korayem, A.M. Shafei, Application of recursive Gibbs–Appell formulation in deriving the equations of motion of N-viscoelastic robotic manipulators in 3D space using Timoshenko beam theory, Acta Astronautica, 83 (2013) 273-294.
[27] M.H. Korayem, A.M. Shafei, F. Absalan, B. Kadkhodaei, A. Azimi, Kinematic and dynamic modeling of viscoelastic robotic manipulators using Timoshenko beam theory: theory and experiment, Int J Adv Manuf Technol, 71 (2014) 1005-1018.
[28] M.H. Korayem, A.M. Shafei, M. Doosthoseini, F. Absalan, B. Kadkhodaei, Theoretical and experimental investigation of viscoelastic serial robotic manipulators with motors at the joints using Timoshenko beam theory and Gibbs–Appell formulation, Proceedings of the Institution of Mechanical Engineers, Part K: Journal of Multi-body Dynamics, (2015) 1464419315574406.
[29] M.H. Korayem, A.M. Shafei, H.R. Shafei, Dynamic modeling of nonholonomic wheeled mobile manipulators with elastic joints using recursive Gibbs–Appell formulation, Scientia Iranica: Transactions B: Mechanical Engineering, 19 (2012) 1092-1104.
[30] M.H. Korayem, A.M. Shafei, E. Seidi, Symbolic derivation of governing equations for dual-arm mobile manipulators used in fruit-picking and the pruning of tall trees, Computers and Electronics in Agriculture, 105 (2014) 95-102.
[31] M.H. Korayem, A.M. Shafei, A new approach for dynamic modeling of n-viscoelastic-link robotic manipulators mounted on a mobile base, Nonlinear Dynamics, 79 (2015) 2767-2786.
[32] M.H. Korayem, A.M. Shafei, Motion equation of nonholonomic wheeled mobile robotic manipulator with revolute–prismatic joints using recursive Gibbs–Appell formulation, Applied Mathematical Modelling, 39 (2015) 1701-1716.
[33] M.H. Korayem, A.M. Shafei, S.F. Dehkordi, Systematic modeling of a chain of N-flexible link manipulators connected by revolute–prismatic joints using recursive Gibbs-Appell formulation, Archive of Applied Mechanics, 84 (2014) 187-206.
[34] M. Förg, F. Pfeiffer, H. Ulbrich, Simulation of unilateral constrained systems with many bodies, Multibody System Dynamics, 14 (2005) 137-154.
[35] H. Gattringer, H. Bremer, M. Kastner, Efficient dynamic modeling for rigid multi-body systems with contact and impact: An O(n) formulation, Acta Mechanica, 219 (2011) 111-128.
[36] D. Tlalolini, Y. Aoustin, C. Chevallereau, Design of a walking cyclic gait with single support phases and impacts for the locomotor system of a thirteen-link 3D biped using the parametric optimization, Multibody System Dynamics, 23 (2009) 33-56.
[37] A.M. Shafei, H.R. Shafei, Oblique impact of multi-flexible-link systems, Journal of Vibration and Control, (2016) 1077546316654854.
[38] H. Zohoor, S.M. Khorsandijou, Dynamic model of a flying manipulator with two highly flexible links, Applied Mathematical Modelling, 32 (2008) 2117-2132.